Realistic Models of a One- and Two-Compartment Rat Cerebellar Purkinje Neuron

Allan D. Coop[1] **and George N. Reeke**
Laboratory of Biological Modelling, The Rockefeller University, 1230 York Ave., New York, N. Y. 10021, USA.

Technical Report: 99.01
http://www.rockefeller.edu/labheads/reeke/techpub.html

[1]Corresponding author, Email: adc@lobimo.rockefeller.edu

Abstract

Computer simulation was employed to explore the discharge behavior of one- and two-compartment models of a cerebellar Purkinje cell in response to climbing fiber and current pulse stimulation. We could not find a unique parameter set for any model that replicated the full temporal detail of reported discharge patterns. However, a new composite model cell gave a better overall match to emperical data than similar models employing the more realistic Hodgkin-Huxley description of conductances. The better match achieved by the simpler models suggests that the composite level of description is well suited to simulation of neuronal discharge patterns and the temporal detail required for the realistic functional exploration of large scale neuronal networks.

Introduction

One of the great challenges for neurophysiology is the description of the mechanisms of temporal integration that subserve the serial order of behavior. Generally, it is assumed that the requisite sequencing functions arise from the elaborate systems of interconnected neurons and neuronal networks that comprise the cerebral cortex (Lashley, 1948; Carpenter et al., 1999) and subcortical systems such as the basal ganglia (Houk, 1997; Wickens, 1997; Redgrave et al., 1999). The cerebellum is also known to play an important role in the timing of behavior (Thompson, 1990; Hauge et al., 1998). An understanding of the mechanisms of temporal pattern recognition and generation requires the analysis of many such networks and their constituent neurons so as to identify their temporal characteristics. Although much insight is available from studies performed *in vivo*, *in vitro*, and with the aid of non-invasive imaging techniques, the ability to construct realistic computational models can greatly facilitate the interpretation of such empirically derived knowledge, both in the case of normal and pathological functions.

The adoption of more realistic models of neurons for the development of neuronal network simulations has increased the difficulty of selecting the level of detail to include in the modelled cells because even the most detailed cell models seem unable accurately to replicate reported discharge behaviors with a single set of parameter values (see for example Fig. 4 Llinás and Sugimori, 1980a c.f. Fig. 5 De Schutter and Bower, 1994a; Fig. 6 Llinás and Sugimori, 1980a c.f. Fig. 9 De Schutter and Bower, 1994a; Fig. 4 Traub et al., 1991; Fig. 3 Traub et al., 1993; Fig. 3 Migliore et al., 1995; Fig. 12.5 Protopapas et al., 1998). The behavior of simplified compartmental models has suggested that reduced models of hippocampal neurons may not be capable of reproducing the exact output of detailed models using identical parameters (compare, for example, Pinsky and Rinzel, 1994 with Traub et al., 1991) but that models of pyramidal neurons may do so within an acceptable range if parameters are adjusted (Jackson and Cauller, 1997). This may also be the case for single compartment models (for example Figs. 3, 4, and 5, Wang, 1999). Further, for single compartment models, even when employing multiple conductances described by the highly realistic Hodgkin and Huxley (1952) equation system (HH), the more specific the range of acceptable behaviors required from a model, the narrower and more non-physiological the regions of the best fit parameter values become, such that attempts to generate a single set of conductance values to match the discharge response of a neuron to both current injection and synaptic activation have failed (Foster et al., 1993). In the case of motoneurons in spinal cord slice cultures the geometric constraints by which a dendritic tree can be reduced to an equivalent cylinder (Rall, 1977) are not met, and attenuation of synaptic currents may be modelled less well in cells with extensive dendritic branching (Ulrich et al., 1994). Such observations suggest that the standard techniques employed for simulating both detailed and reduced model cells may be limited in their applicability.

Nevertheless, there are compelling reasons supporting the development of reduced but realistic models of, for example, a cerebellar Purkinje (PC) neuron. (i) When the number of synaptic inputs and the size and electrical complexity of its dendritic tree are taken into account, this cell type is one of the most complex in the nervous system (Ito, 1984). It is located within the cerebellum, an area known for its involvement in motor activity, and it has been studied at many levels, including the molecular, the physiological, and the behavioral. Insights into the realistic modelling of this cell type at the one- or two-compartment level may apply as well to other less complex cells and ultimately contribute to network models of the temporal evolution of neuronal discharge. (ii) Detailed simulation of PCs suggests that the cable properties of central neurons may be quite different in the freely behaving animal, when background synaptic activity is present, from those reported for slice preparations and anesthetized animals where such activity is much reduced or absent (Rapp et al., 1992). (iii) In part, the attraction of a simple but realistic single compartment model cell lies in the ability to constrain otherwise complex and interdependent non-linear interactions, thus simplifying the interpretation of simulation output. Such an approach is more biologically realistic than that employing the simple summating or leaky-integrator units of artificial and pulsed neural networks (e.g. Hopfield, 1982; Maass and Bishop, 1999) and may be crucial when the temporal dynamics of a network are important.

Several considerations suggest that one- or two-compartment models may be good enough for the simulation of realistic large-scale neuronal networks and, as we show here, may fit experimental data at least as well as detailed multi-compartmental models. (i) In models of three different neocortical neurons, a reduction in the number of compartments by an (average) order of magnitude shortened simulation times by a factor of approximately 17$\times$ (Jackson and Cauller, 1997). It would be expected that a second such reduction (by more than an order of magnitude) to one or two compartments would achieve further computational savings. (ii) Theoretical considerations have suggested that the responses of PCs are independent of the dendritic location of synchronous parallel fiber inputs (De Schutter and Bower, 1994c) and that, more generally, voltage-dependent properties of dendrites may eliminate the location-dependent variability of synaptic activation (Cook and Johnston, 1999). Recent experimental evidence has provided some support for these predictions by showing that active conductances located in complex dendritic trees serve to make the summation of synaptic conductances linear (Cash and Yuste, 1999). (iii) Finally, simplified models allow the influence of pathological states on network behavior to be explored in a much more realistic and detailed manner than in more artificial neural networks and circuits. Most importantly, they allow for the realistic incorporation of subcellular mechanisms that putatively control phenomena such as memory, learning, and conditioned responses (e.g. Bhalla and Fiala et al., 1996; Schweighofer and Arbib, 1998; Iyengar, 1999).

Accordingly, we set out to develop a realistic model PC that could be used in a large-scale simulation of the role of the cerebellum in certain temporal aspects of behavior, and which would also serve as a template for developing models of other cell types in cerebellar and cerebral cortex based on similar principles. Because there was a great deal of confusion in the literature as to the relative merits and regions of validity of the several existing detailed PC models, we decided to construct models incorporating features of these models, but so organized that they could be compared under similar simulation conditions. The method was to select representative data sets from the literature and by computer simulation determine which modelling approaches gave a better match to the temporal evolution of the target data.

Methods

Although in principle all data for realistic modelling should be obtained from the cell being simulated, or at least from the same cell type within the same species, in practice the available empirical data are neither complete nor ideal. It is not unusual for data from different sources to be inconsistent or contradictory. Even when the full morphology of a cell is available, somatic voltage transients produced by a current input to the soma do not allow the unique specification of the biophysical parameters of passive membrane (Rall et al., 1992), and channel conductances measured by contemporary voltage-clamp techniques may only be indicative of active membrane properties (McCormick and Huguenard, 1992; De Schutter and Bower, 1994a). We found the development of even a simple model of a PC was highly underconstrained, particularly with respect to the distribution and density, and consequently the magnitude, of the various membrane conductances identified in these neurons. Nevertheless, we attempted to make our models consistent with as many data as possible and where appropriate we provide justification for the choices made. The extent of uncertainty and inconsistency between the reported behavior of PCs and highly detailed models of both passive and active membrane properties for the guinea-pig (Rapp et al., 1994; De Schutter and Bower, 1994a, respectively) and rat (Shelton, 1985; Bush and Sejnowski, 1991, respectively), the fact that the rat is preferentially used in many electrophysiological and behavioral studies, and the requirement for the simplest possible realistic model cells for incorporation into large network models, led us to explore the discharge behavior of simple one- and two-compartment models of PCs based preferentially on rat PC data.

This section describes four models of a PC located in the cerebellar cortex of the rat. Each model cell was distinguished by either the number of compartments or by the complement of membrane conductances and how they were modelled. Formal descriptions of the various PC models and the HH rate equations that describe each conductance of Models 2 and 4 are given in Appendix A and B, respectively. Unless otherwise stated the parameter values for each model PC are absolute. They are listed in Table 1 for Models 1 and 3, and Table 2 for Models 2 and 4. Unless otherwise given, units are in milliseconds (ms) for time, millivolts (mV) for membrane potential, millisiemens (mS) for conductance, microamperes (μA) for current, microfarads (μF) for cell membrane capacitance, micromoles (μM) for concentration, and square micrometers (μm^2) and cubic micrometers (μm^3) for area and volume, respectively.

Model 1: Single-Compartment Composite Purkinje Cell

Model 1 was the simplest of the model PCs studied. It was intermediate in complexity between a simple leaky integrate-and-fire cell and a more complex multi-compartment cell. It

Table 1: Parameter values for Models 1 and 3, the one and two-compartment composite cells, respectively. Conductances are given as absolute values. Unless otherwise stated, all parameter values employed by Models 1 and 3 are those given here. Abbreviations: AP–action potential, TTP–time-to-peak.

Parameter	**Model 1**	**Model 3**
R_n (MΩ)	38.0	38.0
C_m (nF)	2.63	2.63
f_{Cm}	—	0.5
G_i (nS)	—	50.0
τ_m (ms)	100	100
V_r (mV)	-65	-65
PC discharge threshold (mV)	-53	-53
AP amplitude (mV)	80	80
AP TTP (ms)	1	1
Absolute refractory period (ms)	3.5	3.5
$\bar{g}_{Nap}$ (nS)	2.9	6
$V_{Nap_{th}}$, $V_{Nap_{max}}$ (mV)	-60, -25	-60, -25
$\bar{g}_{Caps}$, $\bar{g}_{Capd}$ (nS)	53, —	3.08, 30.8
$V_{Cap_{th}}$, $V_{Cap_{max}}$ (mV)	-55, -25	-55, -25
$\bar{g}_{leak}$ (nS)	47.6	147
$\bar{g}_{Klump}$ (μS)	2.26	0.9
$\bar{g}_{Klump}$ TTP (ms)	0.5	0.75
$\bar{g}_{sAHP}$ (nS)	3.5	4
$\bar{g}_{sAHP}$ TTP (ms)	100	40
$\bar{g}_{Glu}$ (nS)	255	255
$\bar{g}_{Glu}$ TTP (ms)	5	5
E_{Na} (mV)	50	50
E_{Ca} (mV)	70	70
E_K (mV)	-90	-90
E_{leak} (mV)	-65	-65
E_{Glu} (mV)	0	0

was a composite model implemented as a single compartment RC equivalent circuit. A persistent sodium conductance (g_{Nap}) and a P-type Ca^{2+} conductance (g_{Cap}), each exhibited a threshold for activation and were modelled as instantaneous voltage-dependent conductances. The remaining membrane conductances included a 'lumped' K^+ (g_{Klump}) conductance that combined all K^+ conductances contributing to repolarization of the action potential and the relative refractory period, a leak conductance (g_{leak}), and a slow afterhyperpolarizing conductance (g_{sAHP}). Both g_{Klump} and g_{sAHP} were each modelled as a single alpha function of time (Appendix A, Eq. 3).

In Model 1, either sufficient synaptic activation or current injection depolarized the membrane potential (V_m) until the voltage threshold for activation of the persistent currents was reached. Depolarization first activated g_{Nap} then g_{Cap} and, once activated, these two conductances increasingly augmented membrane depolarization. As a numerical simplification, at the threshold for cell discharge the time course of the action potential was imposed by the addition of a precalculated increment to V_m at each time step. This incremental depolarization was chosen to match the peak membrane depolarization typical of a PC impulse. In contrast to the reset of V_m to the resting membrane potential (V_r) typically employed for leaky integrator models of cell discharge, here g_{Klump} was activated during cell discharge to repolarize V_m. If present, g_{sAHP} was also activated at this time. Simultaneously, an absolute refractory period was initiated which prevented the model cell from discharging for a time that limited the cell discharge frequency to the maximum reported for PCs. By its control of the magnitude and time-to-peak of the fast afterhyperpolarization g_{Klump} also controlled the duration of the relative refractory period.

Model 2: Single-Compartment HH-Based Purkinje Cell

In Model 2 the simplified dynamics of the conductances employed in Model 1 were replaced by the HH formalism. Ionic currents included a fast (I_{Naf}–De Schutter and Bower, 1994a) and a persistent (I_{Nap}–Kay et al., 1998) sodium current, a high-threshold P-type Ca^{2+} current (I_{Cap}–De Schutter and Bower, 1994a; Regan, 1991), an anomalous rectifier (I_{Kh}–Spain et al., 1987), an A current (I_{Ka}–Wang et al., 1991), a delayed rectifier and a noninactivating K^+ current (I_{dr} and I_{Km}, respectively–Yamada et al., 1998), and a large (BK-type) and low-threshold (K2-type) Ca^{2+}-activated K^+ current (I_{Kc} and I_{K2}–Yoshida et al., 1991; De Schutter and Bower, 1994a, respectively).

In this model the Nernst potential for the Ca^{2+} conductance was computed at each time step (Hille, 1992). Intracellular Ca^{2+} was assumed to be buffered by a fixed uniform unsaturable Ca^{2+} buffer that bound Ca^{2+} instantaneously. The absence of mobile Ca^{2+} buffers was justified on the grounds that their inclusion would unnecessarily complicate calculations and was not warranted on the basis of the many other approximations made and the uncertainty of many of the necessary parameters. The assumption that binding was instantaneous was considered reasonable as it occurs within 20–40 μs (using parameter values of Klingauf and Neher, 1997 in Eq. [20] of Wagner and Keizer, 1994). The Ca^{2+} buffering constant (B) was initially set to 4700 (Llano et al., 1994). A simple scheme similar to that given by McCormick and Huguenard (1992) was used to convert I_{Cap} to an intracellular Ca^{2+} concentration ($[Ca^{2+}]_i$). When $[Ca^{2+}]_i$ was required (Models 2 and 4), the concentration was adjusted to reported values by varying the volume assumed for the intracellular Ca^{2+} shell volume (v_i).

Model 3: Two Compartment Composite Purkinje Cell

Model 3 extended the complexity of Model 1 by introducing a second compartment to allow independent evolution of somatic and dendritic membrane potentials. The conductances and their implementation were the same as those of Model 1 with the addition of an axial conductance (G_i) that described the coupling between the two compartments. A value for this parameter was derived by estimating G_i between the soma and the spiny dendrites from data given by Shelton (1985), according to $G_i = \pi r^2/R_i l$ (where l is the segment length, r the segment radius, and R_i the axial resistance, $R_i = 150\,\Omega$cm, Spruston and Stuart, 1996), to give a value of approximately 83.3 nS (or 12 MΩ). Although it is considered difficult to ascribe precise morphological correlates to the compartments of a two compartment model,

Table 2: Parameter values for Models 2 and 4, the one and two compartment Hodgkin-Huxley (HH) based cells, respectively. Appendix B gives parameter values for the HH rate equations employed. Conductances are given as absolute values for the surface areas indicated by the index and given in Table 3. With the exception of E_{Ca} values for the reversal potentials were as given in Table 1. For Models 2 and 4, the appropriate choice of $\bar{g}_{Cap}$, v_i, v_d, B_s, B_d and calculation of the Nernst potential for E_{Ca} at each time step gave a reduction of E_{Ca} to 70 mV during the action potential. Unless otherwise stated, all parameter values employed by Models 2 and 4 are those given here.

Parameter	**Model 2**	**Index**	**Model 4**	**Index**
C_m (nF)	2.63	A0	2.63	A0
G_i (nS)	—	—	83.3	—
f_{Cm}	4.8	—	2	—
v_i, v_d (μm^3)	0.1	—	0.25, 0.5	—
B_s, B_d	4,700	—	470, 4,700	—
$\bar{g}_{Naf}$ (μS)	46.8	S0	81.9	S0
$\bar{g}_{Nap}$ (pS)	25.7	S0	25.7	S0
$\bar{g}_{Cap}$ (nS)	14.6	S3	16.2, 530	S3, D2
$\bar{g}_{Kh}$ (nS)	25.7	S0	7.0, 34.5	S0, S1
$\bar{g}_{Kdr}$ (μS)	14.0, 3.5	S0, S1	7.0	S0
$\bar{g}_{Km}$ (nS)	0.936, 1.15, 0.0324	S0, S1, S2	7.0, 34.5	S0, S1
	4.19, 14.3	D0, D1	4.19, 14.3	D0, D1
$\bar{g}_{Ka}$ (nS)	351, 230	S0, S1	351, 1,730	S0, S1
$\bar{g}_{Kc}$ (μS)	1.87	S1	4.6	s1
$\bar{g}_{K2}$ (nS)	126	D0	16,100	D0
E_{Ca} (mV)	142	—	142	—

we initially followed Llano et al., (1991) and made the simplifying assumption that the soma, the smooth dendrites, and their associated thorns formed one compartment and the spiny dendrites and spines the other. For convenience these two compartments are referred to below as the 'somatic' (s) and 'dendritic' (d) compartments, respectively. The distribution of the conductances between the two compartments was a free parameter of the model explored by simulation and reported in the Results. This division of the model PC required the surface area of the cell to be estimated so as to properly distribute the passive membrane parameters R_n and C_m and the various conductances between the two compartments. The surface areas we used are given in Table 3 and we now describe how they were estimated.

The reported total lengths of the spiny and smooth dendrites of three representative rat PCs stained by the Golgi method are reasonably similar (Palay and Chan-Palay, 1974; Shelton, 1985). We employed the values reported by Shelton (1985) for dendritic length and average segment diameter in our estimate of the total surface area of the smooth and spiny dendrites and spines. In comparing the estimates of the smooth, spiny, and total dendritic length for rat and guinea-pig PCs, it was noted that the spiny dendrites of the guinea-pig were approximately 17% shorter than those of the rat, whereas the smooth dendrites were approximately 48% longer than in the rat, although the total dendritic length varied by only about 4% (Palay and Chan-Palay, 1974; Shelton, 1985; Rapp et al., 1994). We preferred the

Table 3: Estimate of the surface area of a rat Purkinje neuron. See Methods for details. The index is employed to refer to a particular compartment in the text and Tables 1 and 2.

Anatomical compartment	**Surface area (μm^2)**		**Index**
Dendritic spine heads	106,000		D3
Dendritic spine necks	110,000		D2
Total dendritic spines		**216,000**	D1
Spiny dendrites		**32,200**	D0
Thorn heads	324		S4
Thorn necks	335		S3
Total thorns		**660**	S2
Smooth dendrites		**11,500**	S1
Soma		**2,340**	S0
Total		**263,000**	A0

value of 1.25 μm^2 for the surface area of a single spine (Napper and Harvey, 1988) because it made allowance for tissue shrinkage, whereas estimates of 1.1 (Shelton, 1985) and 1.12 μm^2 (Harris and Stevens, 1988) did not and indeed the two smaller estimates corresponded well to Napper and Harvey's uncorrected values. Given the mean number of spines (173,000), their longitudinal dendritic density (17.4/μm) and surface area (Napper and Harvey, 1988), and a representative spiny dendritic length for the rat PC, the total surface area of the spines and spiny dendrites was calculated to be 248,000 μm^2.

Each PC is also contacted by a single CF (Cajal, 1911) that make a total of 512 ± 50 synaptic contacts (Silver et al., 1998) with a ratio of one synapse per thorn (Palay and Chan-Palay, 1974). Knowing the mean length, head and shaft diameters (Palay and Chan-Palay, 1974) of a representative thorn allowed its contribution to the surface area of a PC to be estimated at 0.653 μm^2, or 333 μm^2 for all thorns. Table 3 shows that the total surface area of our representative PC (263,000 μm^2) was approximately 1.75–2.2× that of the 119,000–150,000 μm^2 typically employed by previous models of guinea-pig PCs (De Schutter and Bower, 1994a; Rapp et al., 1994; Shelton, 1985).

Model 4: Two Compartment HH-Based Purkinje Cell

In Model 4 the simplified conductances of Model 3 were replaced with the more detailed HH description. The channel types incorporated into Model 4 were the same as those employed by Model 2. The Ca^{2+} buffering constant B was assumed to be 470 and 4700 in the soma and dendrites, respectively (Llano et al., 1994, and above).

Other Model Parameters

The V_r of PCs has been reported to vary widely (-50 to -70 mV, Jaeger and Bower, 1994; Stuart and Häusser, 1994). Unless otherwise stated,we set V_r to -65 mV for each of our model PCs (c.f. -66.7 $\pm$ 2.4 mV, Llinás and Sugimori, 1980a; -63.9 $\pm$ 8.3 mV, Jaeger and Bower, 1994). In the composite models (Model 1 and 3) we set the discharge threshold to 12 mV depolarized from V_r (estimated from Stuart and Häusser, 1994). Unless otherwise stated, the spike amplitude measured from V_r was adjusted to 80 mV (c.f. 74.9 ± 5.6 mV, Llinás and Sugimori, 1980a; 90 ± 3.5 mV estimated from Fig. 2A Stuart and Häusser, 1994). The membrane time constant (τ_m) for the composite models (Model 1 and 3) was assumed to be 100 ms (based on Rapp et al., 1994). The maximum value for each of the conductances ($\bar{g}$) was based on those given by De Schutter and Bower (1994a) and Bush and Sejnowski (1991). These values were then varied to find an acceptable match with reported behavior of the PC cell membrane under several protocols including Na^+ channel block by tetrodotoxin (TTX) and Ca^{2+} channel block by cobalt (Co^{2+}). These target pharmacological protocols were mimicked by removal from the model cells of Na^+ or Ca^{2+} and Ca^{2+}-activated K^+ conductances, respectively. Because ultimately we want to study the temporal evolution of neuronal discharge, where possible we chose to focus on the subthreshold and discharge behavior of PCs, rather than simpler characterizations of cell behavior such as the experimental f/i (frequency vs. current pulse magnitude) plot. However, when f/i relationships could be plotted, the slope was calculated for comparison with the empirical range of 48–234 Hz/nA estimated from Figure 5B of Llinás and Sugimori (1980a). For the K^+-associated properties of the model cells, the target values were obtained from Figure 6A–C of Llinás and Sugimori (1980a), from which we estimated the test current pulse magnitudes to be 0.3, 0.5, 1.0, and 1.7 nA and the target membrane depolarizations to be 6.3, 10.5, 18 and 20 mV, respectively. For the short (80 ms) current pulse simulations the empirical profiles were taken from Figure 4A–D of Llinás and Sugimori (1980a), whereas for CF-initiated discharge the empirical profiles were the spontaneous PC discharges illustrated in Figure 1C of Llinás and Sugimori (1980a) and for slow afterhyperpolarization (sAHP), Figure 1A and Table 1 of Hashimoto and Kano (1998). For convenience, empirical profiles for the CF, pharmacological, current pulse responses, and f/i relationships are given in Figure 1. Also included in this figure are the discharge profiles of a highly detailed multi-compartment PC model (De Schutter and Bower, 1994a). We based the conductances incorporated into our model cells on those given by De Schutter and Bower, but excluded the low threshold T-type Ca^{2+} conductance as it is considered to disappear during normal PC development (Usowicz et al., 1992). Absolute conductances were calculated on the basis of the areas given in Table 3 and are given for the composite and HH models in Tables 1 and 2, respectively. We preferred this approach to that of a single value for each type of conductance as it allowed different conductance magnitudes to be employed for the surface areas of different anatomical parts of the cell.

The temperature dependence of channel kinetics was assumed to exhibit a Q_{10} factor of 3 (Hodgkin and Huxley, 1952). Therefore, the rate constants from Yamada et al. (1998) (I_{Kdr}, I_{Km}) and Regan (1991) (I_{Cap}) were increased from room temperature to 37 °C by a factor of 5. The temperature dependence of g_{Nap} was not modelled.

In each model cell the multiple excitatory synaptic contacts made by the CF that contacts a single PC (Palay and Chan-Palay, 1974; Eccles et al., 1966) were modelled as a single alpha function of time. We allowed for the likely temporal spread of CF-initiated excitatory postsynaptic potentials at these synapses by giving the conductance a time-to-peak of 5 ms.

Regan (1991) gave the peak I_{Cap} in dissociated PCs as 1986 pA at -20 mV with Ba^{2+} replacing Ca^{2+} as the charge carrier. The peak Ca^{2+} current was reported as 42 % of the peak Ba^{2+} current, allowing the peak I_{Cap} to be estimated at 0.83 nA for 7–21 day postnatal rats. In 8-10 day rats (Llano et al., 1994), peak dendritic $[Ca^{2+}]_i$ was 685 nM in response

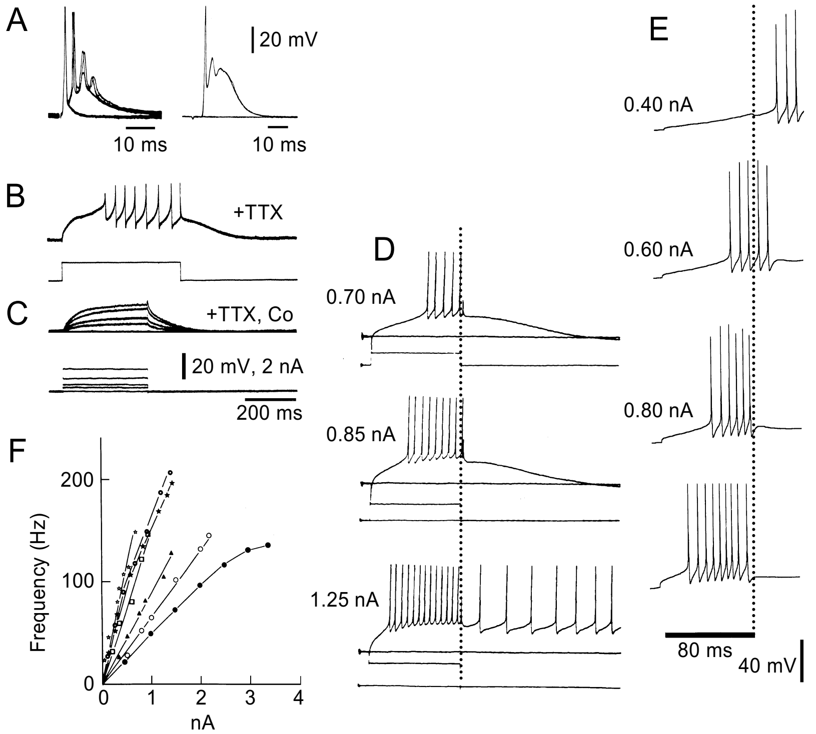

Figure 1: The four model PCs were tuned to match the target profiles A–D and F illustrated in this figure. A, B, C, D and F were adapted from Figs. 1, 6, 4 and 5 of Llinás and Sugimori (1980a). E was adapted from Fig. 5 of De Schutter and Bower (1994a) and illustrates the discharge response of a detailed 1,600 compartment PC to different current pulse magnitudes. The vertical (dotted) lines in D and E indicate the end of the current pulse. The critical feature illustrated in D is that spontaneous PC discharge occurred only after the end of a 1.25 nA current pulse. The scale bars in E also apply to D.

to a 20 ms depolarization to 0 mV, a value 7× that of the soma, and the maximum Ca^{2+} current was 8 nA of which 70-90 % was I_{Cap}. Under these circumstances I_{Cap} was estimated at 6.4 nA. With the aid of the simplifying assumptions that $[Ca^{2+}]_i$ was proportional to I_{Cap} and I_{Caps} was 1/7 that of I_{Capd} we calculated an I_{Caps} of 0.91 nA which compared favorably with the value of 0.83 estimated above from Regan (1991). Consequently, we initially chose target values of 0.87 (I_{Caps}) and 6.0 nA (I_{Capd}) for the two-compartment, and an I_{Cap} of 6.87 nA for the one-compartment PC models. In some simulations, the value of I_{Cap} was scaled in proportion to the magnitude of injected current.

It was also found necessary to introduce a membrane capacitance scaling factor (f_{Cm}) to permit adjustment of the total membrane capacitance (C_m) of a cell. In the one-compartment HH Model 2 f_{Cm} had the effect of reducing the apparent surface area of the cell membrane. Without this adjustment factor it was not possible to increase $\bar{g}_{Naf}$ to generate cell discharge with a spike depolarization that matched the required target amplitude without inducing spontaneous PC discharge. In the case of the two-compartment models, f_{Cm} was the proportion of C_m apportioned to the somatic compartment when C_m was distributed between the somatic and dendritic compartments.

In an effort to maintain a low computational overhead, the numerical solution of the various equation systems was implemented with difference equations. Simulation timesteps were set to 5 or 10 μs for the HH and composite models, respectively. We considered that any limitations of this approach were outweighed by the number of assumptions and approximations required to fully describe each model cell.

Tuning the Model Purkinje Cells

The discharge behavior of each model cell was explored using computer simulations to identify a parameter set or sets that replicated the reported passive membrane properties of a PC as well as active responses to either synaptic drive by an impulse in a single climbing fiber (CF) or to different magnitudes of somatic current injection. There were several reasons for focusing our study on synaptic activation of PCs by the CF. The identification of a unique parameter set that simultaneously accommodated both the rapid membrane response to such a large synaptic event and the much slower and smaller rates of depolarization in response to current pulse stimulation for the cell geometries studied provided a considerable challenge for the two modelling approaches employed. We did not explicitly study parallel fiber activation of PCs as we considered the continuous asynchronous stimulation provided by this source to be encompassed by current pulse stimulation. Further, parallel fiber discharge implies the discharge of inhibitory stellate and basket cells that together converge at PCs to generate complex sets of synaptic activation that involve a variety of temporal relations explored in the context of a local circuit network rather than in an "isolated" PC, the latter being a case that has been studied in some detail (De Schutter and Bower, 1994b; Jaeger et al. 1997; Jaeger and Bower, 1999).

Simulations proceeded by selecting sets of V_m traces from the literature (the empirical profiles) and 'tuning' the model PCs by trial and error to give the best obtainable match. The aim was to identify a unique set of parameter values for the two stimulation paradigms that satisfied the more physiological CF stimulus by generating a complex spike (CS). For this reason we began tuning each cell by matching its discharge response to CF activation. The detailed tuning of each PC in response to the pharmacological protocols continued after identification of these parameter sets. Although at the outset we hoped this approach would allow us to develop an efficient tuning protocol (see for example Foster et al., 1993; Segev and Burke, 1998), we generally found that tuning benefited by randomly varying the order of the tuning procedures between tuning for current injection or synaptic activation while employing the best parameter sets from previous matches for the various cell models. After exploring the behavior of the single compartment models, studies were extended to two-compartment cells once the limitations of the putatively more realistic HH-based models became apparent.

After observing many simulations, we noted that, particularly for the case of the HH models, certain conductances appeared to dominate in the control of V_m over certain voltage ranges and/or in the control of a particular component of membrane behavior. For example, the anomalous potassium conductance (g_{Kh}) provided the most direct control of V_r, the persistent Na^+ conductance (g_{Nap}) controlled the rate of membrane depolarization in response to current injection, the BK-type Ca^{2+}-activated potassium conductance (g_{Kc}) provided a more powerful control of membrane repolarization than the K^+ delayed rectifier (g_{Kdr}), and the K2-type Ca^{2+}-activated K^+ conductance (g_{K2}) controlled the time course of plateau depolarization. We employed such assumptions to simplify the searching of parameter spaces and were supported in this approach by previous observations that also attributed putative functions to individual ionic conductances (Llinás, 1988; Storm, 1990).

Tuning in the case of the pharmacological protocols typically proceeded by adjustment of the maximum leak conductance ($\bar{g}_{leak}$) in the composite models, or C_m, the maximum persistent potassium conductance ($\bar{g}_{Km}$), or a somatic leak conductance ($\bar{g}_{leak}$) in the HH model, and the maximum P-type high-threshold calcium (Ca^{2+}) conductance ($\bar{g}_{Cap}$) in all models. In the case of the HH models, alterations in K^+ conductances generally required a change in $\bar{g}_{Kh}$ to return V_m to the required V_r. PC discharge behavior was then matched to the empirical current pulse profiles. Here, $\bar{g}_{Nap}$ was altered in the composite, and in the HH models an initially small $\bar{g}_{Naf}$ was incremented until an action potential with the appropriate amplitude was generated. The sets of parameter values so identified were then tested for their response to a single CF impulse. In Models 2 and 4 $\bar{g}_{Cap}$ was then fine tuned along with v_i to give physiological magnitudes for I_{Cap}, $[Ca^{2+}]_i$, and the Ca^{2+} reversal potential (E_{Ca}). These were approximately 0.9–7.0 nA for I_{Cap}, 10 μM for total $[Ca^{2+}]_i$ (De Schutter and Bower, 1994a), and 70 mV for E_{Ca} (Regan, 1991). Iterative tuning of conductance magnitudes between the two stimulation paradigms (current injection and synaptic activation) was then adopted to identify final parameter values. Once a model PC was tuned, simulations were rerun with representative parameter sets to generate the data for the Figures. Further details of PC tuning are reported where appropriate in the Results section.

Results

Model 1: One-Compartment Composite Purkinje Cell

Initially, we examined the relation between the uniform passive membrane properties of our model PC and reported values for the rat (Jaeger and Bower, 1994) and the guinea-pig (Rapp et al., 1994) for the membrane resistance (R_n) of PCs in the presence of caesium (Cs^+) ions and under 'normal conditions'.

From our estimate of the total average area of a PC (Table 3, A0) and an assumed membrane capacitance of 2.63 nF (1 $\mu F/cm^2$, Shelton, 1985; Cole, 1968) and time constant (τ_m) of 100 ms, the R_n of the model PC was calculated to be 38 MΩ, a value that was larger than the reported value for the guinea-pig of 28.7 MΩ in the presence of Cs^+. However, if only the surface area of the soma, smooth and spiny dendrites, and thorn and spine necks (Table 3–S0, S1, D0, S2 and D2, respectively, or 0.6 of the total surface area) was assumed to contribute to the membrane area of the model PC, R_n was calculated to be 22.8 MΩ. This value was in very good agreement with the reported *in vivo* value of 23.0 MΩ for the rat PC (Jaeger and Bower, 1994). This supported our estimates of the total surface area of the model PC and its passive membrane properties.

A large number of preliminary simulations showed that PC discharge was quite sensitive to the choice of the length of the absolute refractory period and the magnitude of the spike repolarizing conductance g_{Klump}. The magnitude of the absolute refractory period was eventually set to 3.5 ms, a period during which PC discharge was prevented. This limited the maximum frequency of PC discharge to approximately 285 Hz, a value about 1.4× that of the highest frequencies of PC discharge illustrated in the empirical relationships (Fig. 1F). It was then relatively straightforward to choose a representative value for $\bar{g}_{Klump}$ such that during current injection it was large enough to prevent cell discharge at the maximum discharge frequency (set by the absolute refractory period), but not so large that it prevented the frequency of PC discharge scaling in a plausible manner with the magnitude of the current pulse.

In Model 1 the threshold of g_{Nap} was set to -65 mV and its magnitude to 2.9 nS (Kay et

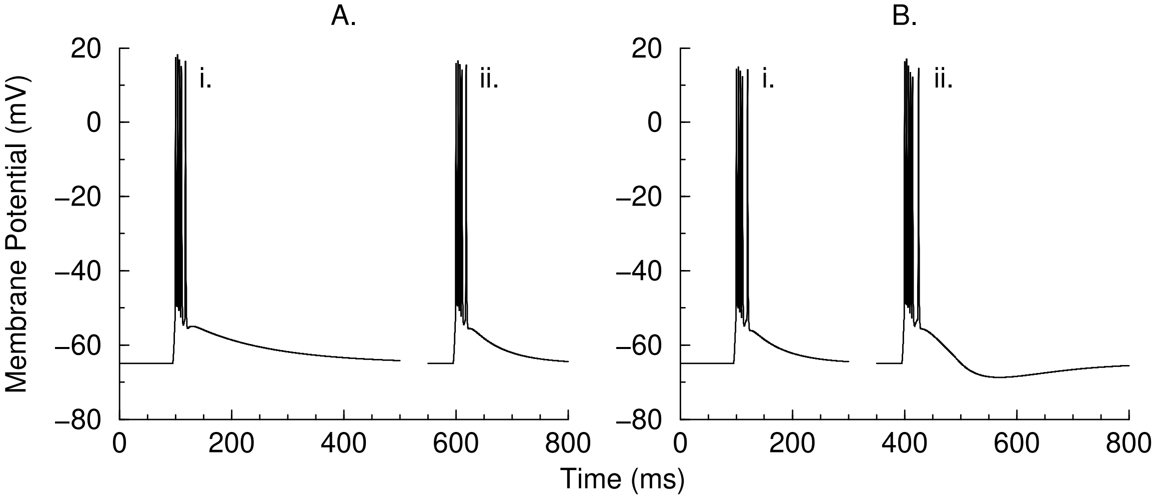

Figure 2: The effect of CF activation on the single-compartment composite PC model (Model 1). Ai: PC discharge after the initial tuning but prior to detailed tuning, $\bar{g}_{leak}$: 25.6 nS, $\bar{g}_{Nap}$: 2.9 nS. Aii: When $\bar{g}_{leak}$ was doubled to 51.2 nS the duration of the ADP was greatly reduced. Bi: Reducing $\bar{g}_{Cap}$ from 53 to 7.8 nS had little influence on the PC discharge profile. Bii: An increase in $\bar{g}_{Nap}$ to 29 nS and the addition of a 3.7 mV slow afterhyperpolarization that peaked approximately 170 ms after the first impulse (Hashimoto and Kano, 1998), extended the period of the ADP but reduced the membrane time constant to approximately 50 ms. All other parameter values are given in Table 1.

al., 1998) and the threshold of g_{Cap} to -55 mV (Llinás and Sugimori, 1980b). The magnitude of $\bar{g}_{Cap}$ was then set to generate an I_{Cap} of 6.9 nA. Under these simulation conditions, PC discharge in response to a single CF impulse gave a reasonable match to the empirical response by generating an initial action potential followed by four impulses and an afterdepolarization (ADP) of about 10 mV (Fig. 2Ai). In these simulations the number of impulses in the CS was most easily controlled by the time-to-peak of the CF synaptic conductance (g_{Glu}), which for this model was set to 5 ms. Doubling $\bar{g}_{leak}$ from 25.6 to 51.2 nS reduced τ_m (calculated as the time taken for V_m to relax to 1/e of the peak ADP) by about half (from 148 to 65 ms, Fig. 2Bii) but had no influence on the number of impulses generated.

Tuning of the model PC was continued by matching its discharge behavior to that given for the empirical pharmacological protocols. Under the conditions of +TTX and +Co, $\bar{g}_{leak}$ was scaled to give membrane depolarizations in response to different magnitudes of current pulse that matched the empirical depolarizations. When $\bar{g}_{leak}$ was doubled from 25.6 to 51.2 nS the model PC gave a good match to the empirical profiles for current pulse magnitudes of 0.3 (5.7 c.f. empirical 6.3 mV), 0.5 nA (9.5 c.f. empirical 10.5 mV), and 1.0 nA (19 c.f. empirical 18 mV) (Fig. 3A). To match the empirical membrane depolarization of 20 mV for a current pulse of 1.7 nA required $\bar{g}_{leak}$ to be increased by a factor of 3.5× to 89.6 nA (2× scaling illustrated, not this result). Here we note that increasing $\bar{g}_{leak}$ by factors of 2× or 3.5× had the effect of decreasing R_n from 38 to 19.5 or 11.2 MΩ, respectively.

Membrane depolarizations of the model PC were then matched to those of the empirical pharmacological protocol of +TTX block of I_{Naf} and I_{Nap} (Fig. 1B). When $\bar{g}_{Cap}$ was set to 7.8 nS an I_{Cap} of 0.74 nA generated a 40 mV depolarization. However, under these simulation conditions the model PC did not discharge calcium spikes in response to a 460 ms 1.37 nA

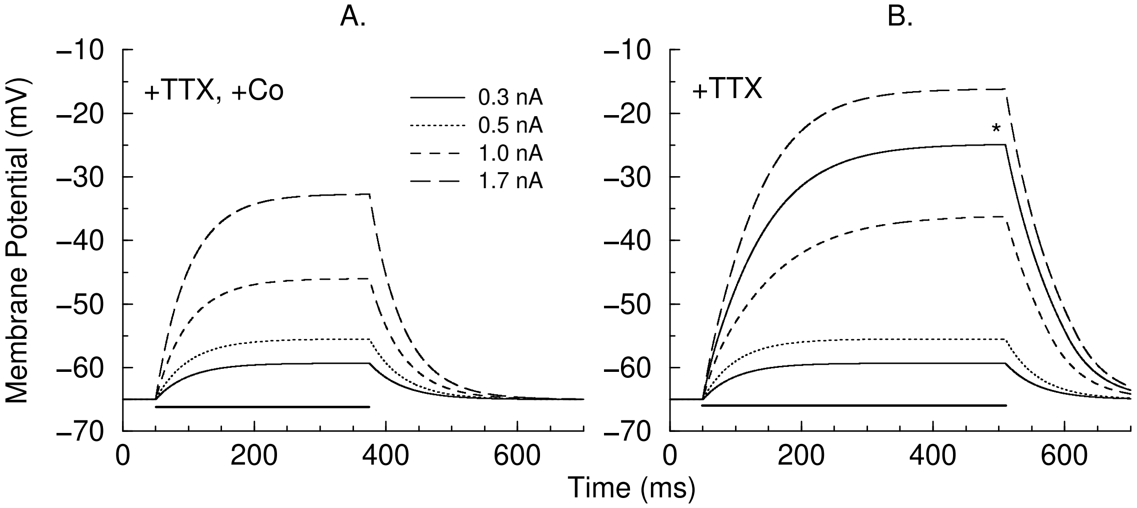

Figure 3: The membrane properties of Model 1 were matched to those reported by Llinás and Sugimori (1980a) under conditions that mimicked the pharmacological conditions of +TTX and +Co. A: Better matches to the reported profiles were achieved by doubling the leak conductance to 51.2 nS. B: A calcium conductance ($\bar{g}_{Cap}$) of 7.8 nS gave a good match to the maximum membrane depolarization reported for the +TTX condition, but failed to generate calcium spikes (profile indicated by the asterisk). The legend in A giving the magnitudes of the current pulses also applies to B. The horizontal bar indicates the 325 (A) or 460 (B) ms period of the current pulse. All other parameter values are given in Table 1.

current pulse (Fig. 3B, trace indicated by asterisk).

After plausible membrane properties for the model PC were established by tuning under the pharmacological protocols, the response of the cell to 80 ms current pulses of different magnitudes was explored. The aim of these simulations was to match the discharge patterns of the model PC to reported empirical profiles (see Fig. 1D) while employing the parameter values identified under the previous pharmacological protocols. At any one magnitude of current injection there were only two parameters available in Model 1 for advancing the discharge time of the first impulse, $\bar{g}_{Nap}$ and/or $\bar{g}_{Cap}$. Simulations showed that changes in $\bar{g}_{Nap}$ had the greater influence on the time to first impulse as g_{Nap} was activated by any depolarization from V_r. By comparison with g_{Nap}, g_{Cap} was only activated by a depolarization greater than 10 mV, therefore it exerted only a limited influence on sub-threshold fluctuations of the membrane potential over the 2 mV between its threshold and the threshold for cell discharge. However, once activated, g_{Cap} had a greater influence on the frequency of PC discharge than g_{Nap} as it was typically a larger conductance and its reversal potential (E_r) was 20 mV more depolarized than that of g_{Nap}.

With the set of parameter values identified by the initial tuning of the CF response and refined by tuning under the pharmacological protocols, the model PC discharged a single impulse 58.6 ms after the onset of a 0.85 nA current pulse (c.f. empirical delay of 33 ms). An increase in $\bar{g}_{Cap}$ by an order of magnitude to 78 nS advanced the discharge time of the first of three impulses by a further 5.4 ms (53.2 ms after current onset). Alternatively, an increase in $\bar{g}_{Nap}$ by an order of magnitude (to 29 nS) initiated the first of four PC impulses 32.6 ms after current onset and generated spontaneous discharge at a frequency of 17.3 Hz following

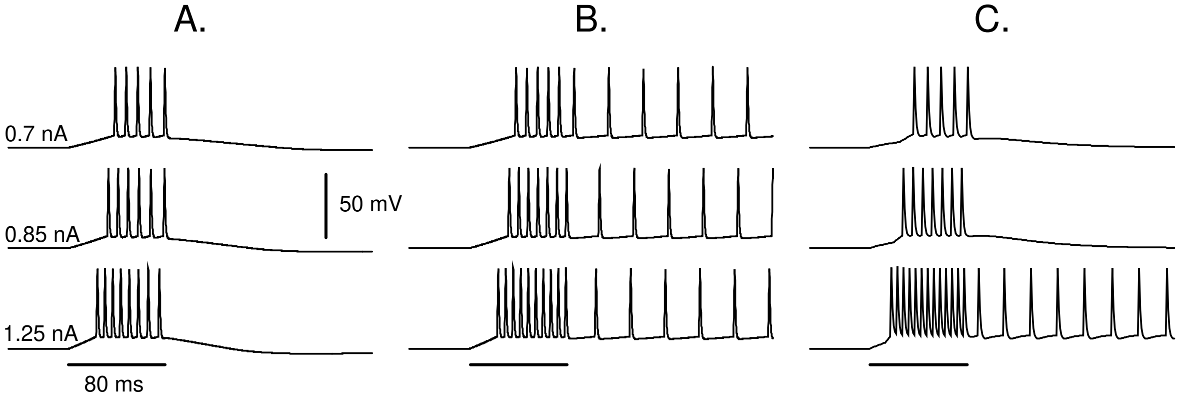

Figure 4: The discharge behavior of Model 1 in response to 80 ms current pulses of different magnitude. A: PC discharge under the +sAHP condition with $\bar{g}_{Nap}$ set to 29 nS, $\bar{g}_{Klump}$ 2.17 μS, and other parameter values as given in Table 1. With this parameter set the PC only discharged during a current pulse. B: When the sAHP was removed the model PC discharged spontaneously following the current pulse at a frequency of approximately 35 Hz. C: When g_{Cap} was simulated as an instantaneous conductance change with exponential decay, activated at the peak depolarization of the action potential, and I_{Cap} was scaled by the magnitude of the injected current, the discharge response of the model PC gave a very good match to the target profiles (Fig. 1D). The vertical and horizontal scale bars given in A also apply to B and C.

termination of the current pulse. Under these conditions the maximum I_{Cap} observed was 1.02 nA and occurred when V_m was +7.7 mV. A reduction in $\bar{g}_{Nap}$ from 29 to 20 nS eliminated the spontaneous PC discharge but was still sufficient to initiate a persistent plateau depolarization that stabilized at a V_m 9.9 mV depolarized from V_r (i.e. marginally smaller than the threshold for g_{Cap}). A simultaneous increase in $\bar{g}_{Cap}$ by an order of magnitude advanced PC discharge by 1.4 ms and generated two initial impulses followed by a further four at a discharge frequency of about 80 Hz. These changes had little influence on the plateau depolarization which was still maintained following the current pulse.

With $\bar{g}_{Nap}$ and $\bar{g}_{lump}$ set to 29 nS and 2.17 μS, respectively, 5, 7 and 10 impulses were generated during current pulses of 0.7, 0.85, and 1.25 nA, respectively. Under these conditions, the PC discharged spontaneously at approximately 35 Hz after the end of the current pulse (Fig. 4B). Spontaneous discharge was eliminated by introducing a slow afterhyperpolarization (sAHP) with an amplitude of 3.7 mV that peaked approximately 169 ms after the first PC impulse (Fig. 4A, sAHP from Hashimoto and Kano (1998). Under these conditions τ_m was about 50 ms (Fig. 2Bii).

Figure 4C illustrates a very good match with the behavior reported in response to current injection that was obtained only when I_{Cap} was modeled as an instantaneously activated current proportionately scaled by the magnitude of the current pulse and exhibited an exponential decay (see Discussion). However, in the one-compartment model this result was extremely sensitive to the choice of $\bar{g}_{lump}$ and $\bar{g}_{Nap}$.

The influence of the sAHP on the discharge behavior of the model PC in response to different magnitudes of current injection is shown by the f/i curves plotted in Figure 5A ($\pm$ sAHP). When $\bar{g}_{Klump}$, $\bar{g}_{Nap}$, and $\bar{g}_{Cap}$ were set to 2.17 μS, 29 nS, and 7.8 nS, respectively,

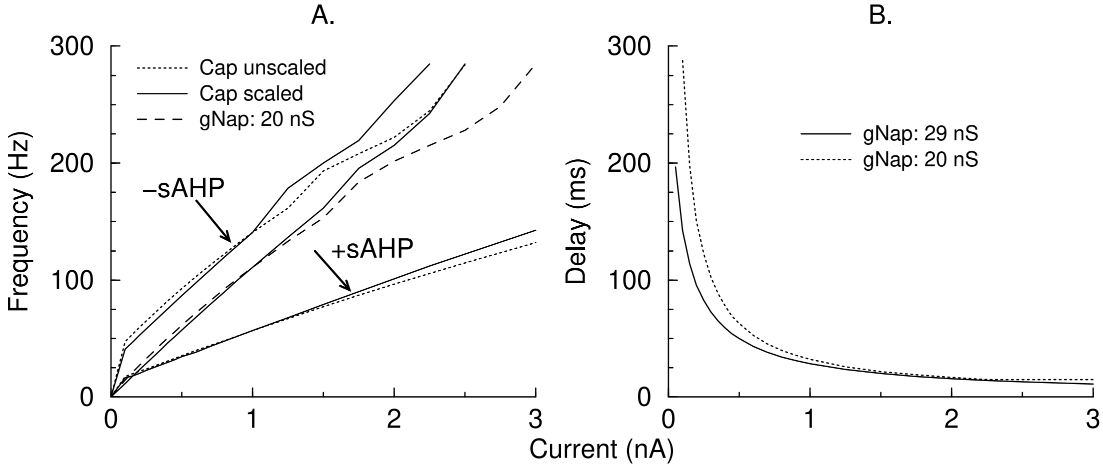

Figure 5: Relationship of discharge frequency and the magnitude of injected current (f/i relationship) for Model 1. A: The influence of a sAHP and/or scaling I_{Cap} in proportion to the magnitude of the current pulse on the f/i relationship, $\bar{g}_{Nap}$: 29 nS. Scaling g_{Cap} tended to linearize the f/i relation, particularly for the -sAHP condition. Under this condition, f/i curves (unscaled: 94 Hz/nA, scaled: 112 Hz/nA) were within the range of the target response (48–234 Hz/nA) illustrated in Figure 1F. In the +sAHP condition PC discharge was reduced (unscaled: 40 Hz/nA, scaled: 44 Hz/nA). Also shown is the effect of reducing $\bar{g}_{Nap}$ from 29 to 20 nS. This had little influence on the f/i relation (90 Hz/nA). B: Delay between the onset of current injection and discharge of the first impulse versus the magnitude of injected current. Reducing $\bar{g}_{Nap}$ from 29 to 20 nS delayed the time of the first impulse following current onset for current magnitudes < 1.5 nA. Discharge frequency was calculated within the period of the 460 ms current pulse.

f/i values (the change in frequency per nA injected current) ranged from 40–94 Hz/nA for the +sAHP and -sAHP conditions respectively. Here the +sAHP f/i value was lower and the -sAHP f/i value was within the estimated empirical range (48–234 Hz/nA). Simulations were also employed to explore the effect of proportionate scaling of I_{Cap} (see Methods) on the f/i relation of PC discharge. This scaling tended to linearize the f/i relation by slightly reducing the PC discharge frequency for current pulses smaller than 1 nA, while increasing it for values larger than 1 nA, an effect much greater in the absence of the sAHP. This scaling had little influence on either the f/i value (44 and 112 Hz/nA for the +sAHP and -sAHP conditions respectively) or the delay between current onset and the first PC impulse at small amplitudes. However, a reduction in $\bar{g}_{Nap}$ from 29 to 20 nS (-sAHP condition) delayed the time to first impulse with little influence on the f/i relation (110 Hz/nA). Here we note that when the threshold for g_{Nap} activation was increased the initiation of PC discharge required an increase in the magnitude of the current pulse.

Model 2: One-Compartment HH-Based Purkinje Cell

As was the case for Model 1, simulations were initially employed to identify a parameter set for which Model 2 responded to CF synaptic activation with a CS. Following the establishment of a stable V_r (approximately -65 mV) with the full complement of conductances present $\bar{g}_{Naf}$ was increased until the spike amplitude was 80.6 mV, similar to that of the empirical

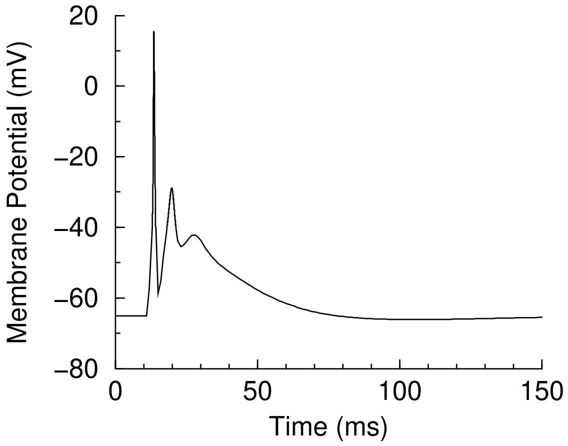

Figure 6: The effect of CF activation on the single-compartment HH-based PC model (Model 2). Cell discharge is shown when it was assumed that the surface area of the model cell was equivalent to the soma, smooth dendrites, thorns, and spiny dendrites (f_{Cm}: 0.17), i.e. the spines did not contribute to the membrane capacitance. In this simulation $\bar{g}_{Kdr}$ was 6.9 μS.

value (80 mV depolarized from V_r). Here we note that in the one-compartment composite PC just described, the spike amplitude following depolarization to the discharge threshold was represented by the addition of fixed increments to V_m. However, in the one-compartment HH-based model (Model 2) the magnitude of $\bar{g}_{Nap}$ was considered to be a free parameter as it ranges from 937 pS–176 μS (calculated as absolute values assuming the somatic compartment size given in Table 3–S0, from 40–7,500 mS/cm^2 Bush and Sejnowski, 1991; De Schutter and Bower, 1994a, respectively). For the PC discharge illustrated in Figure 6 it was assumed that the C_m charged by CF activation was equivalent to the soma, smooth dendrites, thorns, and spiny dendrites or 0.17 of the total surface area of the cell (f_{Cm}:0.17), i.e. the spines did not contribute. Under these conditions, when $\bar{g}_{Naf}$ was increased to 46.8 μS (2,000 mS/cm^2), spike depolarization reached 15.6 mV. With the parameter values given in Table 2 the time course of the discharge profile and the subsequent ADP were similar to that illustrated for the empirical profiles (Fig. 1A).

We next explored the response of the model PC to current injection under the pharmacological protocols. To match membrane depolarization to the empirical profile for a 1.7 nA current pulse under the +TTX and +Co condition required a decrease in $\bar{g}_{Kdr}$ (the K^+ conductance that had the greatest influence on PC depolarization under these conditions). However, the greatest change was the large increase in C_m required to slow the rising phase of the membrane response to the current pulse and generate a monotonically increasing depolarization for the duration of the current pulse. A good match was obtained with a C_m of 12.6 nF (4.8 μF/cm or a f_{Cm} of 4.8×). Under these simulation conditions, there was a reasonable match with the empirical values for membrane depolarization by the model PC, 8.0 (c.f. empirical 6.3 mV), 11.4 (c.f. empirical 10.5 mV), 16.9 (c.f. empirical 18.0 mV), and 20 mV (c.f. empirical 20.0 mV), for pulse magnitudes of 0.3, 0.5, 1.0, and 1.7 nA (Fig. 7A).

With the set of parameter values identified during the previous +TTX, +Co tuning protocol, under the condition of +TTX alone we were unable to find a parameter set that generated Ca^{2+} spikes in the model PC during current injection. However, when $\bar{g}_{Cap}$ was set to 14.6 nS

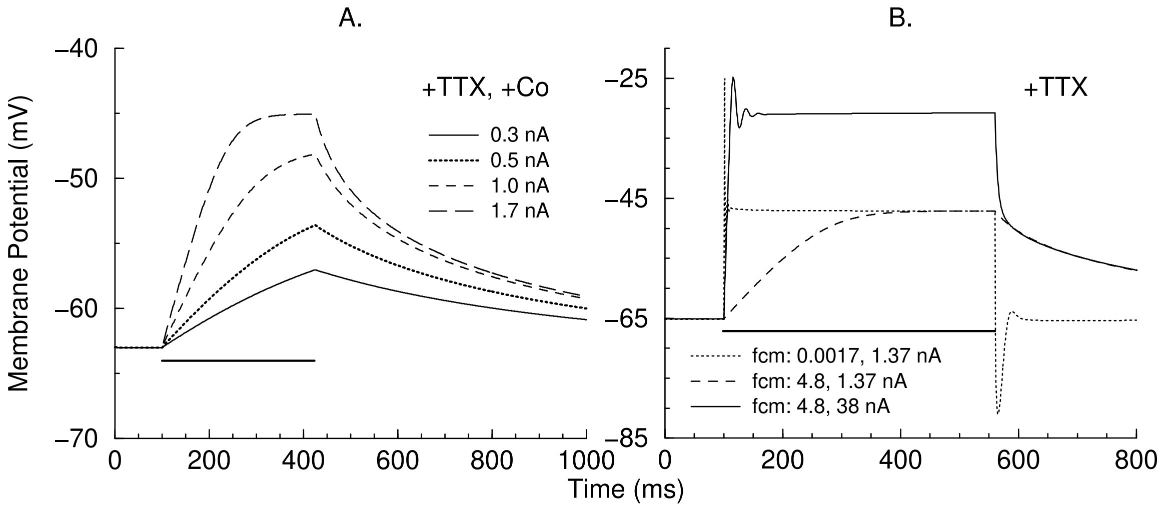

Figure 7: The effect of current injection on Model 2. A: Cell membrane depolarization for four different magnitudes of current pulse when C_m was multiplied by an f_{Cm} of 4.8×. These simulations were performed under conditions that mimicked the pharmacological conditions of +TTX and +Co, i.e. only the non-Ca^{2+}-activated K^+ conductances were active. B: Membrane depolarization under the +TTX condition. In these simulations only g_{Naf} and g_{Nap} were absent. The horizontal bars indicate the 325 and 460 ms durations of the current pulses in A and B, respectively.

and f_{Cm} reduced to 0.0017 we obtained a peak depolarization of the model PC membrane similar to that observed for the equivalent empirical profile (depolarization by approximately 40 mV to -25 mV, in response to a 1.37 nA current pulse, Fig. 1B, TTX). Here we note that this f_{Cm} value scales the total surface area of the PC to give an apparent membrane area of 450 μm^2. This value is between that of the total surface area of the thorn heads (324 μm^2) and the thorns (659 μm^2). Under these conditions, the model PC typically generated a single impulse almost immediately following current onset. This impulse was followed by two or three small amplitude oscillations at a depolarized potential (in this case about -47 mV) that was determined by the magnitude of the injected current. An increase in f_{Cm} to 4.8 slowed the rate of membrane depolarization to give a profile similar to those observed under the +TTX and +Co pharmacological conditions. Increasing the magnitude of the current pulse from 1.37 to 38 nA restored the previous response but with the membrane depolarized to about -30 mV for the period of the current pulse and a with larger post-impulse membrane oscillation (Fig. 7B). We were unable to explore the response of the model PC to current injection under the +Co condition (Ca^{2+}-activated currents blocked by Co^{2+}) because the cell membrane failed to repolarize in the absence of the strong hyperpolarizing influence otherwise provided by the Ca^{2+}-activation of g_{Kc}.

Following detailed tuning, the response of the model PC to prolonged (460 ms) current pulses was explored with f_{Cm} set to 0.17 under normal conditions (i.e. all conductances present). In this case I_{Cap} averaged 0.94 nA, $[Ca^{2+}]_i$ 10.6 μM, and E_{Ca} 70 mV for the impulses following the second impulse generated during a 1.25 nA current pulse (Fig. 8A). Omitting the C_m adjustment given by f_{Cm} slowed cell discharge and reduced the mean spike amplitude by almost 30 mV (51.5 mV depolarization from V_r), However, this had little influence on I_{Cap}, $[Ca^{2+}]_i$, or E_{Ca}, which averaged 0.96 nA, 10.5 μM, and 70.2 mV, respectively (Fig. 8B). Under these conditions, when $\bar{g}_{Naf}$ was increased (to more than 468 μS) to return

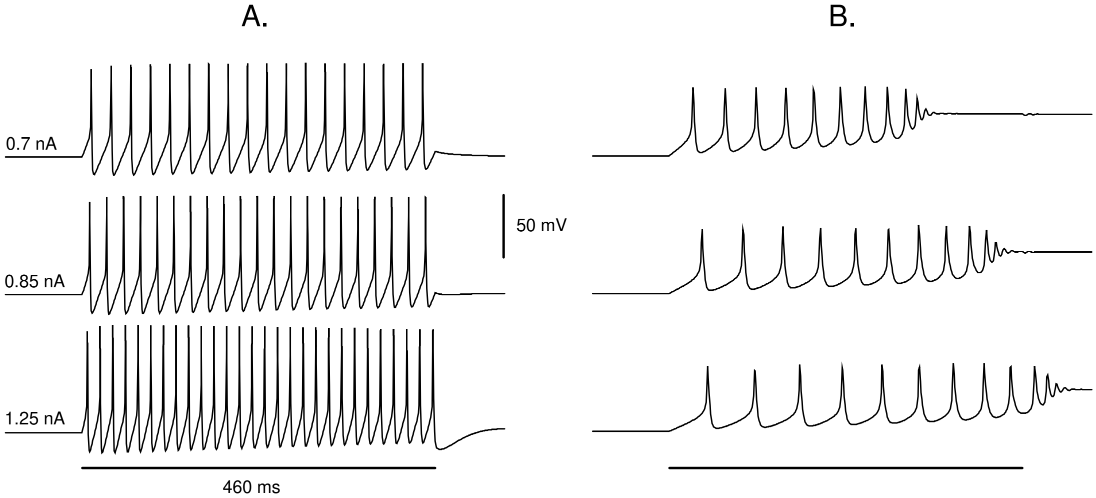

Figure 8: The effect of current injection on Model 2. Cell membrane depolarization for different current pulse magnitudes under two conditions. A: As for Figure 6 C_m was multiplied by an f_{Cm} of 0.17. B: C_m was unmodified. Note both the reduced spike depolarization during the current pulse and the failure of V_m to return to V_r after the end of the current pulse. Current pulse duration was 460 ms (indicated by the horizontal bar), and its magnitude is given is given at the start of each record in A.

the spike amplitude to the empirical value of 80 mV, the model PC discharged spontaneously prior to the start of the current pulse.

Generally, simulations showed that discharge of the full model PC was quite realistic with f_{Cm} set to 0.17, but the most plausible response of the cell with Na^+, Ca^{2+}, and Ca^{2+}-activated K^+ channels blocked (the pharmacological conditions of +TTX and +Co) required f_{Cm} to be set to a value of at least 4.8. In contrast to the discharge behavior of PCs illustrated in the empirical profiles (Fig. 1D), we could not find a parameter set that either delayed the discharge of the first impulse of the model PC or that generated Ca^{2+} spikes during a current pulse.

Model 3: Two-Compartment Composite Purkinje Cell

The addition of a second compartment to the composite model required definition of the anatomical correlates of the two compartments to determine how the CF synapses were distributed between them. Because the CF is known to make synaptic contacts with the thorns of the smooth dendrites, we initially assumed that it only synapsed with the somatic compartment. In this case, reducing G_i from 83.3 to 50 nS improved the match of the model PC discharge profile with the empirical profiles by reducing the number of impulses generated by CF activation. However, this configuration did not generate sufficient dendritic depolarization (typically only about 12 mV) to markedly activate g_{Capd} during the CS. The alternative was an increase in the proportion of CF connectivity with the dendritic compartment. Figure 9A illustrates the effect on PC discharge of varying the location of CF activation between the (i) somatic and (ii) dendritic compartments. Note the long time course (several hundred milliseconds) of membrane relaxation to V_r after the ADP in both cases. In the absence of a specific rationale for locating CF activation we distributed it equally between the somatic

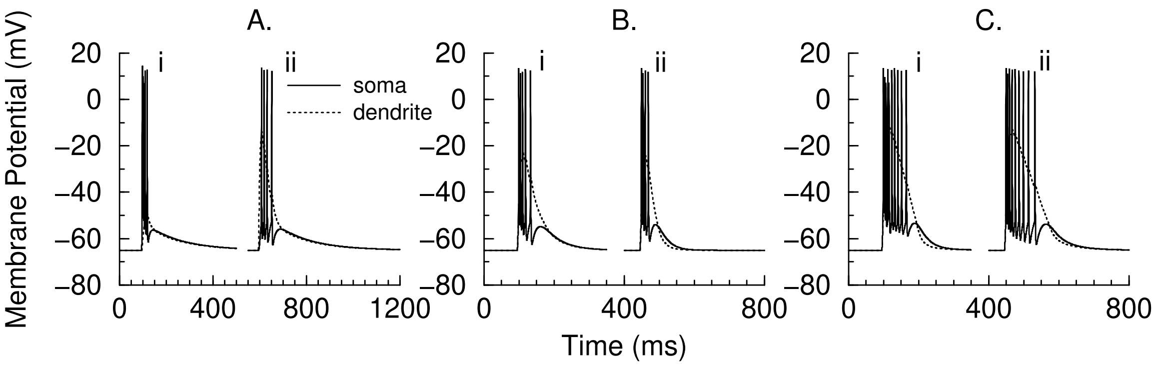

Figure 9: The effect of CF activation on the two-compartment composite PC model (Model 3). The membrane potentials in the somatic and dendritic compartments are indicated by solid and dotted lines, respectively. A(i): CF activation located at the somatic compartment compared to A(ii): CF located at the dendritic compartment. There is a much larger dendritic depolarization in this case. $\bar{g}_{Nap}$ 2.9 nS, $\bar{g}_{Cap}$ 0.45 and 4.5 nS in the soma and dendrites, respectively. B(i): With the CF distributed equally between the somatic and dendritic compartments, increasing $\bar{g}_{leak}$ by a factor of 2.4× to 61.3 nS shortened the period of the ADP, and B(ii): addition of a sAHP further reduced the time course of the ADP. C: The influence of g_{Klump} on CF activation of the PC after detailed tuning of the conductances, (i) g_{Klump} 0.8 nS, (ii) g_{Klump} 0.9 nS.

and dendritic compartments. The discharge response of the model PC was further improved by setting f_{Cm} to 0.5. This made the somatic compartment equivalent to the soma, smooth dendrites, thorns, spiny dendrites, and 77 % of the spine necks. The other parts of this figure will be referred to later below.

We then tuned the membrane depolarization of the model PC in response to current pulse stimulation to those of the +TTX and +Co empirical pharmacological protocols (Fig. 1C). Increasing $\bar{g}_{leak}$ by a factor of 2.4× effectively reduced R_n from 38 to 15.8 MΩ and gave good matches to the smaller empirical membrane depolarizations of 5.9 (c.f. empirical 6.3 mV), 9.8 (c.f. empirical 10.5 mV), 19.6 (c.f. empirical 18 mV) and 33.4 mV (c.f. empirical 20 mV) (Fig. 10A).

Under the conditions of somatic current injection and +TTX, it was necessary for $\bar{g}_{Capd}$ to be about an order of magnitude larger than $\bar{g}_{Caps}$ so as to generate an I_{Capd} a factor of 7× larger than I_{Caps}. When $\bar{g}_{Caps}$ and $\bar{g}_{Capd}$ were set to 0.8 and 8 nS, respectively, I_{Caps} was 0.076 nS and I_{Capd} 0.690 nS for a total I_{Cap} of 0.77 nA in response to a 460 ms 1.37 nA current pulse. Under these simulation conditions the somatic compartment depolarized to the empirical value of -25 mV (Fig 10B, indicated by asterisk). However, as was the case for the other model PC cells we were unable to find a set of parameter values that generated calcium spiking.

We then explored the discharge behavior of Model 3 in response to short (80 ms) current pulses of different magnitude. With the parameter set identified by the previous tuning protocols the time to first impulse was 38.3 ms in response to an 0.85 nA current pulse and two impulses were generated during the pulse period. Reducing $\bar{g}_{Klump}$ to 0.8μS resulted in the generation of three impulses with a total I_{Cap} of 0.1 nA confined to the soma. Further reductions in $\bar{g}_{Klump}$ resulted in burst discharge at the maximum rate. Because of the low

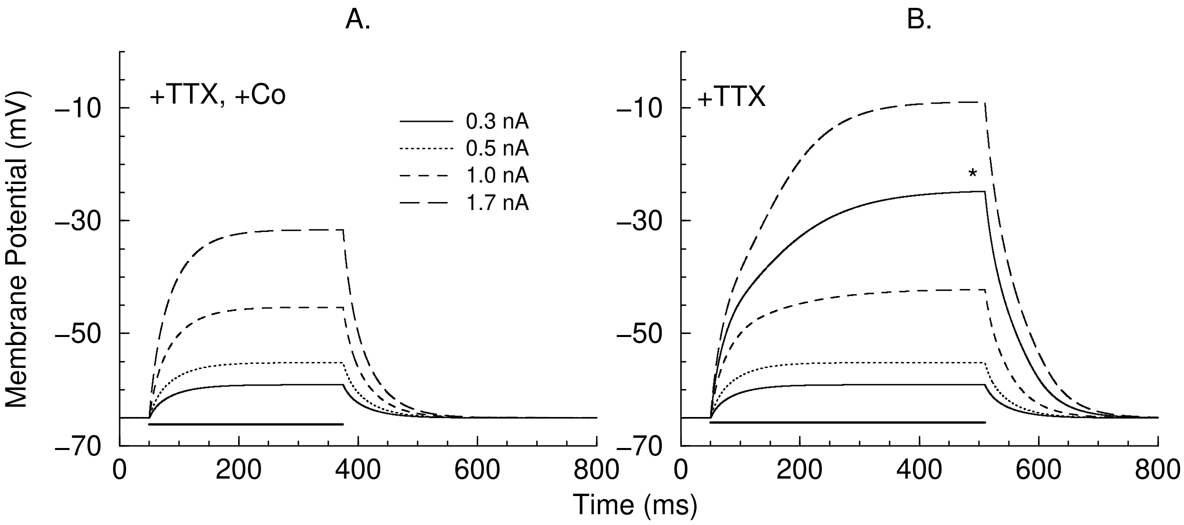

Figure 10: The effect of current injection on Model 3. Cell membrane depolarization in response to current pulses of different magnitude and duration under conditions that mimicked the pharmacological conditions of +TTX and/or +Co block of Na^+ and Ca^{2+} and Ca^{2+}-activated K^+ conductances. A: The set of parameter values that generated the PC response to a CF impulse illustrated in Figure 9B(ii) were tested with the four different current pulse magnitudes given in the legend. In these simulations $\bar{g}_{leak}$ was increased by a factor of 2.4× to 63.2 nS. B: It should be noted that unlike the behavior shown in the target experiment (Fig. 1), the model PC did not discharge Ca^{2+} spikes under the +TTX condition. In these simulations $\bar{g}_{Cap}$ was 0.8 and 8 nS in the soma and dendrites respectively. The horizontal bars indicate the duration of the current pulse of A: 325 and B: 460 ms.

I_{Caps} and absence of I_{CAPd}, $\bar{g}_{Caps}$ and $\bar{g}_{Capd}$ were increased to 3.08 and 30.8 nS in the soma and dendrite, respectively. With these parameter values a train of six spikes generated by an 80 ms 1.25 nA current pulse increased I_{Caps} and I_{Capd} from the first to last spike from 0.35 to 0.37 and 0.54 to 0.94 nA, respectively. Under these conditions the model PC did not exhibit spontaneous discharge after the end of the current pulse (Fig. 11A). However, when I_{Cap} was proportionately scaled by the magnitude of the current pulse there was no change from 0.4 nA for I_{Caps} across six spikes but an increase from 0.0 to 0.9 nA for I_{Capd}. This was a total I_{Cap} of 0.4 and 1.3 nA for the first and last spikes, respectively. Now the model PC discharged spontaneously at an increasing rate (as it should) following the end of a 1.25 nA current pulse (Fig. 11B).

With this parameter set the model PC discharged at the maximum frequency following CF activation. Increasing g_{Klump} from 0.8 to 0.9 μS reduced the period of PC discharge to 80 ms. The addition of a sAHP tuned to allow a total of four impulses in response to CF activation and return the ADP to V_r within 110 ms (see Fig. 9B) reduced the number of impulses to 9 or 10 depending on whether the CF input was located at the dendrite or the soma (Fig. 9C).

We then employed these parameter sets (i.e. ± sAHP and ± proportional I_{Cap} scaling) to explore the f/i relationships of the model PC. The two compartment composite PC cell required a current greater than 0.4 nA to initiate cell discharge. In the absence of the sAHP, the f/i relationship showed a large increase for current pulses larger than 1.25 nA. Similarly, proportional scaling of I_{Cap} had little influence on the f/i relationship until the current pulse was larger than 1.25 nA. However, this scaling ultimately increased the mean f/i value by

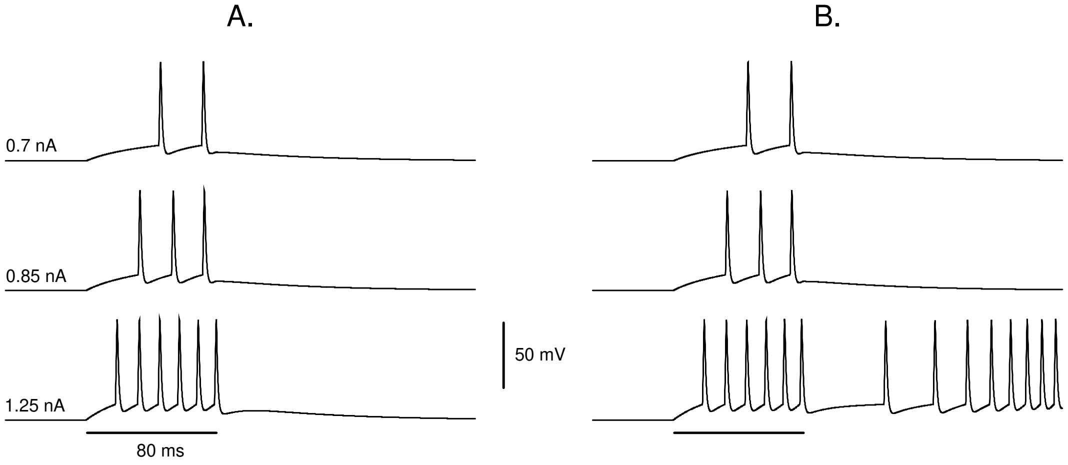

Figure 11: The discharge behavior of Model 3 in response to current pulses of different magnitude. A: Parameter values the same as those used for the CF response illustrated in Figure 9C(i). B: PC discharge profiles after proportional scaling of I_{Cap}. In this case the model PC discharged spontaneously after the end of a 1.25 nA current pulse. The magnitude of the current pulse given at the beginning of each trace in A and the legend also apply to B. The 80 ms period of the current pulse is indicated by the horizontal bar in A and B.

about 20 % (77 to 97 Hz/nA). The rapid increase in the f/i value occurred because once the threshold for g_{Capd} activation was reached large dendritic depolarizations were readily achieved. The addition of the sAHP typically reduced the f/i value by about 50 % and under these conditions proportional scaling of I_{Cap} had little influence (Fig. 12A). In the absence of changes in either $\bar{g}_{Nap}$ or $\bar{g}_{Cap}$ the time to first impulse following current onset was unaffected by changes in the sAHP or proportional scaling of I_{Cap} (Fig. 12B).

Model 4: Two-Compartment HH-Based Purkinje Cell

As with the three previous models, a large number of exploratory simulations were employed to identify a possible set of parameter values for which the two-compartment HH-based PC generated a CS in response to a single CF stimulus.

Similarly to Model 3, it was assumed that the somatic compartment was composed of the soma, smooth dendrites, and thorns or 0.17 of the total surface area of the cell and f_{Cm} was set to this value. PC discharge under the two conditions of all CF activation located at either the (i) somatic or (ii) dendritic compartment is illustrated in Figure 13A. For these simulations the spike amplitude was increased from 80 to 85 mV to increase the CS magnitude, which was quite sensitive to the magnitude of the initial impulse. The time course of the ADP and the number of impulses in the CS were most easily controlled by the relative magnitudes of $\bar{g}_{K2}$ and $\bar{g}_{Capd}$, respectively. Moving the CF input from the somatic to the dendritic compartment increased the total I_{Cap} at the time of peak somatic depolarization by an order of magnitude (0.86 to 12.7 nA) and had an even greater influence on the total I_{Cap} at the time of the peak dendritic depolarization (0.54 to 17.1 nA). Nevertheless, we were unable to find a set of parameter values that matched the temporal details of the CS discharge of the empirical profiles of Figure 1A.

Having established plausible discharge in response to CF activation, we next tried to match PC depolarization to that seen for the empirical pharmacological protocols (Fig. 1B,

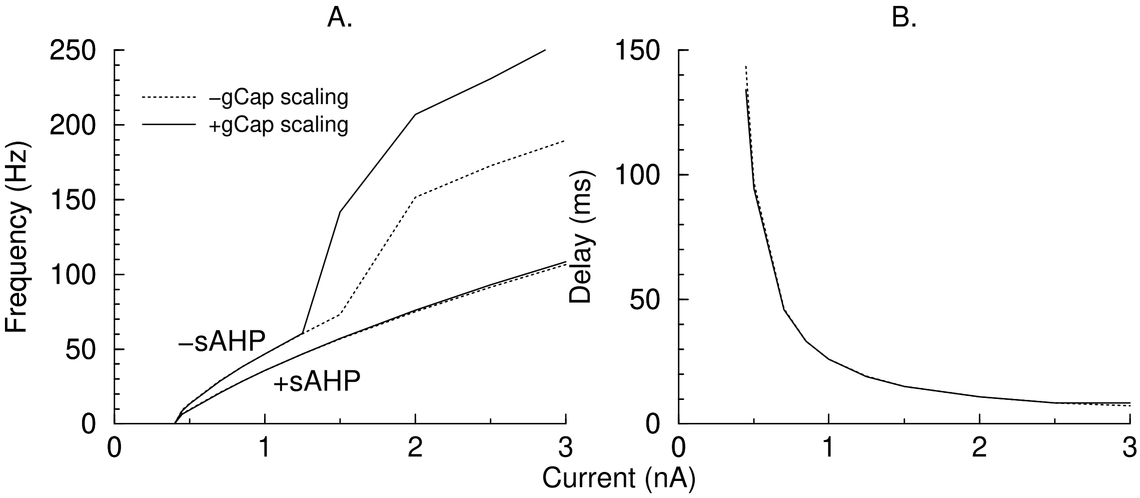

Figure 12: The frequency/current (f/i) relationship of Model 3. A: The f/i relationship is given for the $\pm$ sAHP conditions and proportional scaling of I_{Cap}. The PC discharge frequency was calculated during the period of a 460 ms current pulse. B: The time to first impulse after current pulse onset. Adding either a sAHP or proportional scaling of I_{Cap} had little influence on the occurrence time of the first impulse.

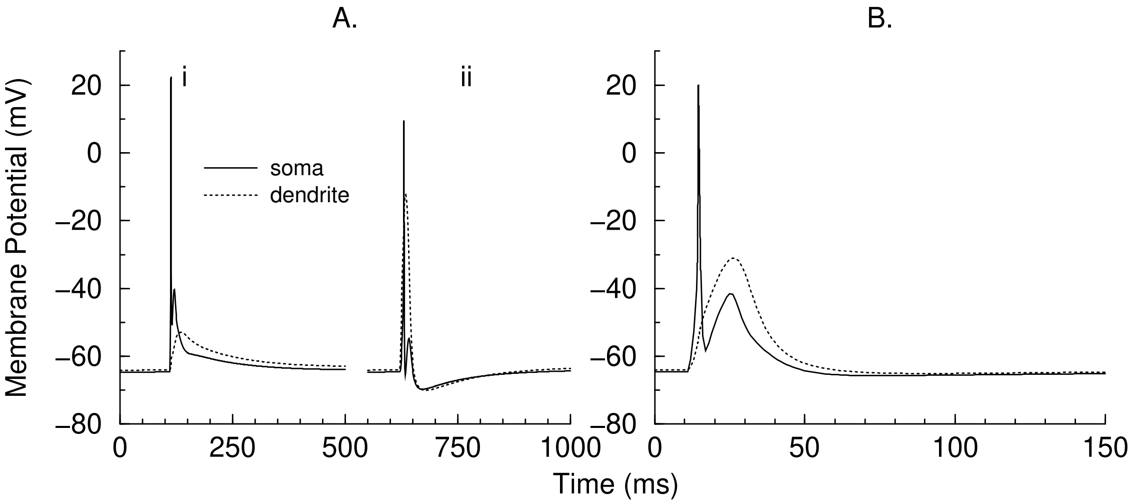

Figure 13: The effect of CF activation on the two-compartment HH-based PC model (Model 4). Cell discharge for three different locations of CF input. A: The surface area of the somatic compartment was the sum of the surface areas of the soma, smooth and spiny dendrites and thorns (f_{Cm}: 0.17), i: CF entirely in the somatic compartment, ii: CF entirely in the dendritic compartment (f_{Cm}: 0.17). Note the large dendritic depolarization and the damped oscillation of V_m. B: CF equally divided between the somatic and dendritic compartments. Note different time scale in A and B. Trace markers in A also apply to B.

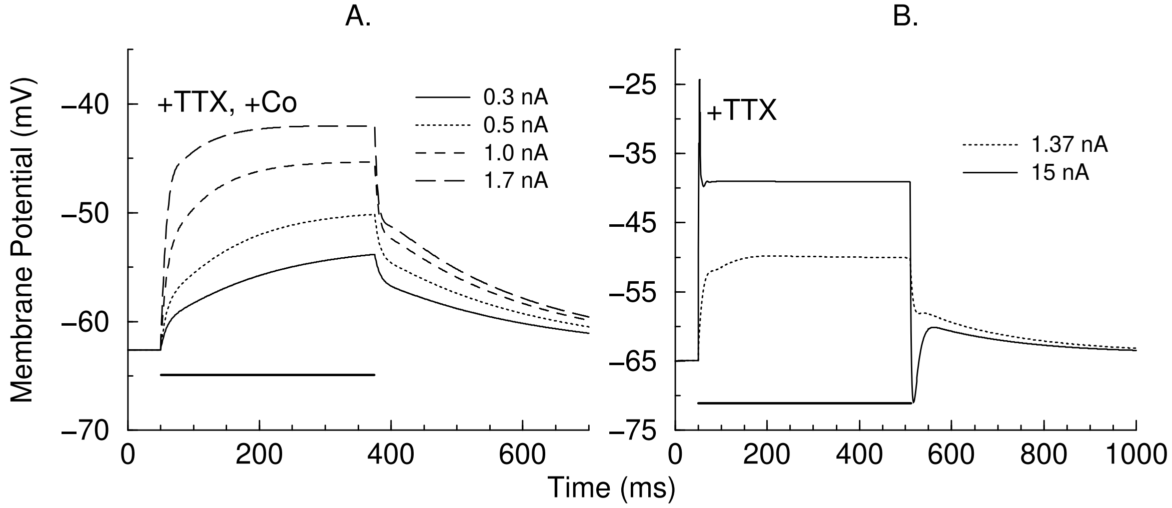

Figure 14: The effect of current injection on Model 4. A: Cell membrane depolarization under simulation conditions that mimicked the pharmacological conditions of +TTX and +Co, i.e. only the non-Ca^{2+}-activated K^+ conductances were present. B: Cell membrane depolarization under conditions that mimicked channel block by TTX only. The horizontal bar indicates the duration of the 325 and 460 ms current pulses in A and B, respectively. In the illustrated simulations it was assumed that the somatic C_m was scaled by a f_{Cm} of 0.17.

C). The response of Model 4 under the conditions of +TTX and +Co is given in Figure 14A. Here, setting f_{Cm} to 2× to generate a monotonically increasing membrane depolarization gave a reasonable match with the empirical profiles. Current pulses of 325 ms and 0.3, 0.5, 1.0 and 1.7 nA gave 8.8 (empirical 6.3 mV), 12.5 (empirical 10.5 mV), 17.3 (empirical 18 mV) and 20.6 mV (empirical 20 mV) depolarizations, respectively (Fig. 14A).

The model PC was then tuned under the pharmacological condition of +TTX alone. In these simulations we found that addition of the Ca^{2+} (g_{Cap}) and Ca^{2+}-activated K^+ conductances (g_{Kc} and g_{K2}) actually reduced the membrane depolarization seen in response to the different current pulses. In the presence of Ca^{2+}, g_{K2} in particular was strongly activated and together with g_{Kc} the hyperpolarizing influence of these two conductances was considerable. We note that the depolarization profile here was similar to that seen for the one compartment HH Model 2 (see Fig. 7B) and it required a current pulse of 15 nA to depolarize the PC membrane to match that of the empirical depolarization. However, as was the case for the other models we were unable to find a set of parameter values that generated the multiple calcium spikes of the empirical profile (Fig. 1B).

We then explored the response of Model 4 to a 80 ms 0.85 nA current pulse. As was the case for Model 2, employing the parameter values identified by the pharmacological tuning protocols resulted in greatly attenuated responses to the test pulse. With f_{Cm} set to 2 an increase in g_{Naf} to 562 μS generated an impulse that depolarized to 13.8 mV 40 ms after current onset. Under these simulation conditions, only two impulses, separated by 43.3 ms, were generated during the current pulse. Similarly, when f_{Cm} was removed, a g_{Naf} of 293 μS generated an impulse that depolarized to 17.8 mV 24 ms after current onset, also with only two impulses generated during the pulse period. Ultimately, we were unable to find a set of parameters based on the tuning protocols that generated a match with the empirical profiles of Figure 1D.

Discussion

We employed computer simulations to examine two different models of membrane conductances in one- and two-compartment simulations of a rat cerebellar Purkinje neuron. The aim was to identify a realistic but simplified model of a geometrically complex neuron and characterize its suitability for inclusion in a large scale neuronal network model. The two models of membrane conductance explored differed in the number of parameters required to describe the conductance in each case. The simpler composite model incorporated membrane conductances, modelled either as voltage-activated alpha functions of time or as linear functions of V_m, into an equivalent circuit that described passive membrane properties. In the composite cells two or three parameters were sufficient to describe time-dependent or persistent conductances, respectively. Alternatively, membrane conductances were described with the HH formalism, an approach traditionally considered to provide a highly realistic description of membrane conductances based on neurotransmitter binding and unbinding rates and channel opening and closing probabilities. This more detailed approach required as many as 10 parameters to describe a single conductance. The method was to determine to what extent and how easily the various model cells we studied could be tuned to match a set of target behaviors chosen from the literature. This approach was based on the assumption that the model(s) that provided the best matches were likely to be the most appropriate for incorporation into large scale neuronal network models.

Here we acknowledge that the composite approach to neuronal modelling by necessity involves simplification of both the spatial and the biophysical properties of a cell. However, it provides a much needed level of detail intermediate to that of the dimensionless point unit or leaky integrator of artificial neural or connectionist networks and that of multi-compartment models. We consider that the composite approach provides both a practical and realistic alternative to the difficulties faced when creating one- and two-compartment cells incorporating the dynamics of HH-type conductances. It remains to be seen to what extent the simplifications it contains affect our ability to model network functions. In this regard, the most significant shortcomings of all the models studied were (i) the reduced representation of detailed current flows in PC dendrites, and (ii) the failure to observe "dendritic" calcium spikes. For the former point, the single compartment models lacked a term that described the axial resistance otherwise available in the two-compartment models. However, it was possible to partially compensate for this deficiency by the introduction of a factor (f_{cm}) that adjusted the apparent C_m and therefore the effective surface area of the cell, and consequently allowed some control over the rate of membrane depolarization in response to current injection. With regard to (ii), the failure to observe calcium spikes was attributed to the lack of explicit thorn and spine geometry in the models.

The exploratory simulations performed prior to detailed tuning showed that it was relatively straightforward to tune each of the four model PCs to generate plausible discharge profiles in response to CF activation (Figs. 2B, 6, 9 and 13B). However, this was not the case when tuning the model cells to the empirical profiles generated by different current pulse protocols. When all parameters values were required to lie within plausible physiological ranges, the putatively more realistic HH-based models failed and we could not find parameter values that allowed the replication of the chosen PC discharge profiles in response to the current pulse protocols employed. More specifically, the problem was the identification of a unique set of parameter values that would both allow appropriate delays in the time of cell discharge and as well generate spontaneous discharge only following the cessation of large magnitude current pulses (see Fig. 1D). Here we note that the results presented by De Schutter and Bower (1994a) for a detailed 1,600-compartment model of a PC displayed an advance in the discharge time of the first impulse with an increase in the magnitude of the injected current, but a *reduction* in the spontaneous discharge with increasing current pulse magnitude (Fig. 1E), similarly suggesting shortcomings in the HH conductance model as employed in their simulations. However, the two-compartment composite model could at least be tuned to give a reasonable match with the empirical data (Fig. 11B).

There are several possible reasons why our current pulse simulations might have failed for the HH-based simulations: (i) A suitable set of parameter values may not have been found because the complete parameter space of each model PC was not searched rigorously. The chances of making this error might be reduced by use of automated parameter search techniques; however, it is not yet clear either how such a search should be conducted or how to be certain that no match is possible when searching fails to find a good match for a particular model (the identifiability problem, Schierwagen, 1994). This is particularly the case where there is doubt as to the appropriate specification of a model that contains a mixture of purely phenomenological and mechanistic elements. This is not just a theoretical issue, as even the most careful conventional analysis can fail to reveal the extreme sensitivity of a model's predictions to the model's underlying structure, parameters, and initial conditions (see for example Wood and Thomas, 1999). Nevertheless, we note that some progress in the development of automated searching techniques has been made (Foster et al., 1993; Tawfik and Durand, 1994; Eichler-West and Wilcox, 1997; Vanier and Bower, 1999) and improved parameter estimation methods for HH models are becoming available (e.g. Willms et al., 1999). The further development and application of such techniques to the present models is beyond the scope of this paper, but we now consider them an essential prerequisite for the identification of reduced HH-based models suitable for incorporation into realistic neuronal network models. (ii) There were many uncertainties associated with the description of several of the conductances included in the HH-based model PCs and not all identified conductances were actually included in the models. This was particularly the case for K^+ conductances (see Gruol et al., 1991). Parameter sets characterizing several of the conductances (primarily the K^+ conductances including, g_{Kdr}, g_{Km}, g_{Ka}, g_{Kh} and g_{Kc}) were either taken from other cell types within the rat or from other species, including invertebrates. Consequently, in many cases there was no valid estimation of either the distribution of conductance density or $\bar{g}$ for the rat PC. (iii) As a phenomenological description of a space-clamped squid giant axon, the HH model may be limited in validity to the quantitative description of currents characterized under the rather artificial conditions of current- or voltage-clamp protocols (see for example Huguenard and McCormick, 1992; McCormick and Huguenard, 1992). Consequently HH models may be more appropriate for the detailed simulation and quantification of single impulses in isolated cells rather than for the complex dynamic patterns of cell discharge associated with the temporal evolution of neuronal behavior under normal conditions. We suggest that this proposition is increasingly supported by a careful examination of the literature. For example, a previous attempt to identify a unique parameter set for both synaptic activation and current pulse in a four-conductance HH model of crustacean walking leg axon also failed for the current injection protocol (Foster et al., 1993); as it did where model behavior and empirical data were explicitly compared (e.g. Vanier and Bower, 1999; Wang, 1999); and the most detailed model of a PC reported to date exhibits several major anomalies when compared to the empirical data it purports to match, particularly with regard to the extent of depolarization during impulse generation (which can be estimated at 147 mV from Fig. 1A, De Schutter and Bower, 1994b). Finally, we note that, although numerous studies have shown shown that the full HH equations provide a comprehensive model of the squid axon, it does not automatically follow that, for reduced neuronal models, combining voltage-clamp equations with cable theory (as first introduced for the spinal motoneuron by Dodge and Cooley, 1977) always gives a valid model (Cronin,1987).

We found the composite Models 1 and 3 to be more successful than the HH Models 2 and 4. In particular, parameter sets were identified for the composite models that generally provided matches to empirical data at least as good if not better than has previously been reported for the two stimulation paradigms employed. This was attributed in part to the greater ease of tuning afforded by the use of just two or three parameters rather than the ten or more required for each conductance in the HH models and the relatively greater independence of these parameters. In the composite models conductance changes were initiated in response to specific events such as cell discharge or activation thresholds. These features allowed the temporal evolution of cell behavior to be treated in a much more discontinuous manner than was possible in the case of the HH simulations with their smoothly varying differentiable functions. We were suprised to find that in many instances the composite models were able to provide a much better match to the reported characteristics of PC behavior than was obtained with a highly detailed multi-compartmental PC model (De Schutter and Bower, 1994a). For example, with an appropriate choice of parameter values (high g_{Nap} and low g_{Cap}) Model 1 generated a nearly linear f/i relation, as did Model 3 over the first 1.25 nA of injected current. This result was quite different from that reported for the multi-compartmental model PC (see Fig. 6B, De Schutter and Bower, 1994a). The introduction of a factor that scaled I_{Cap} in proportion to the amplitude of a current pulse relinearized this relation, a result much more in keeping with the reported f/i behavior (see Fig. 1F). With the appropriate choice of parameter values both composite models exhibited f/i values within the reported range. This result has several interpretations. (i) The proportional scaling of I_{Cap} compensated for the limited spatial properties of the composite models. (ii) Putatively, there was a limited buffer capacity in the real cell such that when the magnitude of a current pulse was small, Ca^{2+} currents were small and I_{Cap} was reduced by Ca^{2+}-buffering mechanisms below the expected magnitude. However, when the magnitude of a current pulse was large, a higher I_{Cap} than expected implied an augmented Ca^{2+} response, possibly a consequence of the combination of Ca^{2+} buffer saturation and Ca^{2+}-activated Ca^{2+} release from intracellular stores (see for example the regenerative signal examined by Llano et al., 1994). (iii) It provides further support for the proposition that active dendritic conductances in combination with the appropriate sub-cellular mechanisms are responsible for the "active linearity" (Cash and Yuste, 1999) that results in a simple input summation arithmetic even for otherwise apparently complex dendritic trees.

Generally, we found the composite approach to the simulation of neuronal behavior to be easier to work with than the HH formalism in the case of one- or two-compartment model cells. This could be attributed to the partitioning of the major effects of conductance changes to particular ranges of membrane polarization. For example, g_{Nap} had its greatest influence between V_r and the discharge threshold, and similarly the greatest effect of g_{Cap} occurred during the action potential. Ultimately, the composite approach may provide a better (or at least more easily tuned) description of the fundamentally discontinuous nature of neuronal mechanisms (see for example McManus and Magleby, 1991, for the BK-type I_{Kc}; Selyanko and Brown, 1999, for I_{Km}) that are subsequently integrated through space and time by the passive properties of the cell membrane than that offered by the assumptions of continuity upon which the HH formalism is based. Because it more closely simulates conductance discontinuities and because of its smaller computational burden, we expect this intermediate composite approach to detailed neuronal modelling to be particularly suited to the simulation of physiologically realistic neurons required for large scale neuronal networks. Such composite models appear to have the twofold benefit of (i) increased functional realism over that of the rate-coded interactions of the leaky integrate and fire model cells typically employed in network simulations with (ii) little increase in computational overhead when compared to the putative advantages of reduced one or two-compartment model cells employing HH-based conductances which have until now been assumed to be highly realistic.

Acknowledgements

Supported by Neurosciences Research Foundation. We would like to thank B. Knight, W. Levick, G. Stuart, and J. Wray for comments. This work was reported in part at CNS*99.

References

Barbour B (1993) Synaptic currents evoked in Purkinje cells by stimulating individual granule cells. *Neuron.* 11:759–769.
Beyer WH (Ed). Handbook of Tables for Probability and Statistics. The Chemical Rubber Co.: Cleveland, Ohio.
Bhalla US, and Iyengar R (1999) Emergent properties of networks of biological signalling pathways. *Science* 283:381–387.
Bush PC, and Sejnowski TJ (1991) Simulations of a reconstructed cerebellar Purkinje cell based on simplified channel kinetics. *Neural Comp.* 3:321–332.
Cajal, S Ramón y (1911) Histologie du Système Nerveux de L'homme et des Vertébrés. II. Malione, Paris.
Carpenter AF, Georgopoulos AP, and Pellizzer G (1999) Motor cortical encoding of serial order in a context-recall task. *Science* 283:1752–1757.
Cash S, and Yuste R (1999) Linear summation of excitatory inputs by CA1 pyramidal neurons. *Neuron* 22:383–394.
Cole KS (1968) Membranes, Ions and Impulses. University of California Press, Berkeley.
Cook EP, and Johnston D (1999) Voltage-dependent properties of dendrites that eliminate location-dependent variability of synaptic input. *J. Neurophysiol.* 81:535–543.
Coop AD, and Reeke GN (2000) Simulating the temporal evolution of neuronal discharge. *Neurocomputing.* In Press.
Crepel F, and Penit-Soria J (1986) Inward rectification and low threshold calcium conductance in rat cerebellar Purkinje cells. An in vitro study. *J. Physiol. (Lond).* 372:1–23.
Cronin J (1987) Mathematical Aspects of Hodgkin-Huxley Neural Theory. Cambridge University Press, Cambridge.
De Schutter E, and Bower JM (1994a) An active membrane model of the cerebellar Purkinje cell. I. Simulation of current clamps in slice. *J. Neurophysiol.* 71:375–400.
De Schutter E, and Bower JM (1994b) An active membrane model of the cerebellar Purkinje cell. II. Simulation of synaptic responses. *J. Neurophysiol.* 71:401–419.
De Schutter E, and Bower JM (1994c) Simulated responses of cerebellar Purkinje cells are independent of the dendritic location of granule cell synaptic inputs. *Proc. Natl. Acad. Sci. USA.* 91:4736–4740.
De Schutter E, and Smolen P (1998) Calcium dynamics in large neuronal models. In: C. Koch and I. Segev, eds. Methods in Neuronal Modeling. 2nd ed. The MIT Press, Cambridge, Mass. pp 211–250.
Dodge FA Jr., and Cooley JW (1977) Action potential of the motoneuron. *IBM J. Res. Develop.*

May:219–229.
Eccles JC, Llinás R, and Sasaki K (1966) The excitatory synaptic action of climbing fibers on the Purkinje cells of the cerebellum. *J. Physiol. (Lond).* 182:268–296.
Eichler-West R, and Wilcox G (1997) Robust parameter selection for compartmental models of neurons using evolutionary algorithms. In: JM Bower, ed. Computational Neuroscience: Trends in Research 1997. Plenum Publishing, New York. pp 75–80.
Fiala JC, Grossberg S, and Bullock D (1996) Metabotropic glutamate receptor activation in cerebellar Purkinje cells as substrate for adaptive timing of the classically conditioned eye-blink response. *J. Neurosci.* 16:3760–3774.
Foster WR, Ungar LH, and Schwaber JS (1993) Significance of conductances in Hodgkin-Huxley models. *J. Neurophysiol.* 70:2502–2518.
Gerstner W, (1999) Spiking neurons. In W. Maass and CM Bishop (Eds). Pulsed Neural Netwotks. MIT Press: Cambridge, Mass. p. 3–53.
Gruol DL, Jacquin T, and Yool AJ (1991) Single-channel K^+ currents recorded from the somatic and dendritic regions of cerebellar Purkinje neurons in culture. *J. Neurosci.* 11:1002–1015.
Harris KM, and Stevens JK (1988) Dendritic spines of rat cerebellar Purkinje cells: serial electron microscopy with reference to their biophysical characteristics. *J. Neurosci.* 8:4455–4469.
Hashimoto K, and Kano M (1998) Presynaptic origin of paired-pulse depression at climbing fibre-Purkinje cell synapses in the rat cerebellum. *J. Physiol. (Lond).* 506:391–405.
Hauge SA, Tracy JA, Baudry M, and Thompson RF (1998) Selective changes in AMPA receptors in rabbit cerebellum following classical conditioning of the eyelid-nictitating membrane response. *Brain Res.* 803:9–18.
Hille B (1992) Ionic Channels of Excitable Membranes. 2nd ed. Sinauer Associates Inc., Sunderland, MA.
Hodgkin AL, and Huxley AF (1952) A quantitative description of membrane current and its application to conduction and excitation in nerve. *J. Physiol. (Lond).* 117:500–544.
Hopfield JJ (1982) Neural networks and physical systems with emergent collective computational abilities. *Proc. Natl. Acad. Sci. USA.* 79:2554–2558.
Houk, JC (1997) On the role of the cerebellum and basal ganglia in cognitive signal processing. *Prog. Brain Res.* 114:543–552.
Hounsgaard J, and Nicholson C (1983) Potassium accumulation around individual Purkinje cells in cerebellar slices from the guinea-pig. *J. Physiol. (Lond).* 340:359–388.
Huguenard JR, and McCormick, AA (1992) Simulation of the currents involved in rhythmic oscillations in thalamic relay neurons. *J. Neurophysiol.* 68:1373–11383.
Ito, M (1984) The Cerebellum and Neural Control. Raven Press, New York.
Jackson ME, and Cauller LJ (1997) Evaluation of simplified compartmental models of reconstructed neocortical neurons for use in large-scale simulations of biological neural networks. *Brain Res. Bull.* 44:7–17.
Jaeger D, and Bower JM (1999) Synaptic control of spiking in cerebellar Purkinje cells: dynamic current clamp based on model conductances. *J. Neurosci.* 19:6090–6101.
Jaeger D, and Bower JM (1994) Prolonged response in rat cerebellar Purkinje cells following activation of the granule cell layer: an intracellular in vitro and in vivo investigation. *Exp. Brain Res.* 100:200–214.
Jaeger D, De Schutter E, and Bower JM (1997) The role of synaptic and voltage-gated currents in the control of Purkinje cell spiking: a modeling study. *J. Neurosci.* 17:91–106.
Kay AR, Sugimori M, and Llinás R (1998) Kinetic and stochastic properties of a persistent sodium current in mature guinea pig cerebellar Purkinje cells. *J. Neurophysiol.* 80:1167–1179.
Klingauf J, and Neher E (1997) Modeling buffered Ca^{2+} diffusion near the membrane: implications for secretion in neuroendocrine cells. *Biophys. J.* 72:674–690.
Koch C and Segev I (eds) (1998) Methods in Neuronal Modeling. (2nd Edn). MIT Press, Cambridge, Mass.
Lashley KS (1948) The problem of serial order in behavior. In: LA Jeffress, ed. (1967) Cerebral Mechanisms in Behavior. Hafner, New York. pp 112–136.
Llano I, DiPolo R, and Marty A (1994) Calcium-induced calcium release in cerebellar Purkinje cells. *Neuron.* 12:663–673.
Llano I, Marty A, Armstrong CM, and Konnerth A (1991) Synaptic- and agonist-induced excitatory currents of Purkinje cells in rat cerebellar slices. *J. Physiol. (Lond).* 434:183–213.
Llinás R. (1988) The intrinsic electrophysiological properties of mammalian neurons: insights into central nervous system function. *Science* 242:1654–1664.
Llinás R, and Sugimori M (1980a) Electrophysiological properties of *in vitro* Purkinje cell somata in mammalian cerebellar slices. *J. Physiol. (Lond).* 305:171–195.
Llinás R, and Sugimori M (1980b) Electrophysiological properties of in vitro Purkinje cell dendrites in mammalian cerebellar slices. *J. Physiol. (Lond).* 305:197–213.
Maass W, and Bishop CM (1999) Pulsed Neural Networks. The MIT Press, Cambridge, Mass.
McCormick AA, and Huguenard JR (1992) A model of the electrophysiological properties of thalam-

ocortical relay neurons. *J. Neurophysiol.* 68:1384–1400.
McManus OB, and Magleby KL (1991) Accounting for the Ca^{2+}-dependent kinetics of single large-conductance Ca^{2+}-activated K^+ channels in rat skeletal muscle. *J. Physiol. (Lond).* 443:739–777.
Migliore M, Cook MEP, Jaffe DB, Turner DA, and Johnston D (1995) Computer simulations of morphologically reconstructed CA3 hippocampal neurons. *J. Neurophysiol.* 73:1157–1168.
Napper RMA, and Harvey RJ (1988) Quantitative study of the Purkinje cell dendritic spines in the rat cerebellum. *J. Comp. Neurol.* 274:158–167.
Palay SL, and Chan-Palay V (1974) Cerebellar Cortex: Cytology and Organization. Springer-Verlag, Heidelberg.
Pinsky PR, and Rinzel J (1994) Intrinsic and network rhythmogenesis in a reduced Traub model for CA3 neurons. *J. Comp. Neurosci.* 1:39–60.
Press WH, Teukolsky SA, Vetterling WT, and Flannery BP (1992) Numerical Recipes in C. Cambridge University Press, Cambridge.
Protopapas AD, Vanier M, and Bower JM (1998) Simulating large networks of neurons. In: I. Segev and C. Koch, eds. Methods in Neuronal Modeling. 2nd ed. MIT Press, Cambridge, Mass. pp 461–498.
Rall W, (1967) Distinguishing theoretical synaptic potentials computed for different soma-dendritic distributions of synaptic inputs. *J. Neurophysiol.* 30:1138–1168.
Rall W, (1977) Core conductor theory and cable properties of neurons. In: Handbook of Physiology. The Nervous System. Cellular Biology of Neurons. Am. Physiol. Soc. Bethesda, MD. sect. 1, vol. I, pp 39–97.
Rall W, Burke RE, Holmes WR, Jack JJB, Redman SJ, and Segev I (1992) Matching dendritic neuron models to experimental data. *Physiol. Revs.* 72:S159–S186.
Rapp M, Segev I, and Yarom Y (1994) Physiology, morphology and detailed passive models of guinea-pig cerebellar Purkinje cells. *J. Physiol. (Lond).* 474:101–118.
Rapp M, Yarom Y, and Segev I (1992) The impact of parallel fibre background activity on the cable properties of cerebellar Purkinje cells. *Neural Comp.* 4:518–533.
Redgrave P, Prescott TJ, and Gurney K (1999) The basal ganglia: a vertebrate solution to the selection problem? *Neuroscience* 89:1009–1023.
Regan LJ (1991) Voltage-dependent calcium currents in Purkinje cells from rat cerebellar vermis. *J. Neurosci.* 11:2259–2269.
Sah P (1996) Ca^{2+}-activated K^+ currents in neurons: types, physiological roles and modulation. *Trends Neurosci.* 19:150–154.
Schierwagen AK (1994) Exploring the computational capabilities of single neurons by continuous cable modelling. *Prog. Brain Res.* 102:151–167.
Schweighofer N, and Arbib MA (1998) A model of cerebellar metaplasticity. *Learning Memory.* 4:421–428.
Segev I, and Burke RE (1998) Compartmental models of complex neurons. In: I. Segev and C. Koch, eds. Methods in Neuronal Modeling. 2nd ed. MIT Press, Cambridge, Mass. pp 93–136.
Selyanko AA, and Brown DA (1999) M-channel gating and simulation. *Biophys. J.* 77:701–713.
Shelton DP (1985) Membrane resistivity estimated for the Purkinje neuron by means of a passive computer model. *Neuroscience* 14:111–131.
Silver RA, Momiyama A, and Cull-Candy SG (1998) Locus of frequency-dependent depression identified with multiple-probability fluctuation analysis at rat climbing fibre-Purkinje cell synapses. *J. Physiol (Lond).* 510:881–902.
Spain WJ, Schwindt PC, and Crill WE (1987) Anomalous rectification in neurons from cat sensorimotor cortex in vitro. *J. Neurophysiol.* 57:1555–1576.
Spruston N, and Stuart G (1996) Voltage attenuation and intracellular resistivity in neocortical pyramidal neurons. Abstract *Soc. Neurosci. Abstr.* 22:792.
Storm JF (1990) Potassium currents in hippocampal pyramidal cells. *Prog. Brain Res.* 83:161–187.
Stuart G, and Häusser M (1994) Initiation and spread of sodium action potentials in cerebellar Purkinje cells. *Neuron* 13:703–712.
Sugihara I, Lang EJ, and Llinás R (1993) Uniform olivocerebellar conduction time underlies Purkinje cell complex spike synchronicity in the rat cerebellum. *J. Physiol. (Lond).* 470:243–271.
Tawfik B, and Durand DM (1994) Nonlinear parameter-estimation by linear association—application to a 5 parameter passive neuron model. *IEEE Trans. Biomed. Eng.* 41:461–469.
Thompson RF (1990) Neural mechanisms of classical conditioning in mammals. *Phil. Trans. R. Soc. Lond. B.* 329:161–170.
Traub RD, Miles R, and Jefferys JGR (1993) Synaptic and intrinsic conductances shape picrotoxin-induced synchronized after-discharge in the guinea-pig hippocampal slice. *J. Physiol. (Lond).* 461:525–547.
Traub RD, Wong RKS, Miles R, and Michelson H (1991) A model of a CA3 hippocampal pyramidal neuron incorporating voltage-clamp data on intrinsic conductances. *J. Neurophysiol.* 66:635–650.
Ulrich D, Quadroni R, and Luscher H-R (1994) Electrotonic structure of motoneurons in spinal cord slice cultures: a comparison of compartmental and equivalent cylinder models. *J. Neurophysiol.* 72:861–871.

Usowicz MM, Sugimori M, Cherksey B, and Llinás R (1992) P-type calcium channels in the somata and dendrites of adult cerebellar Purkinje cells *Neuron* 9:1185–1199.
Vanier MC, and Bower JM (1999) A comparative survey of automated parameter-search methods for compartmental neural models. *J. Comp. Neurosci.* 7:149–171.
Wagner J, and Keizer J (1994) Effects of rapid buffers on Ca^{2+} diffusion and Ca^{2+} oscillations. *Biophys. J.* 67:447–456.
Wang X-J (1999) Fast burst firing and short-term synaptic plasticity: a model of neocortical chattering neurons. *Neuroscience* 89:347–362.
Wang Y, Strahlendorf JC, and Strahlendorf HK (1991) A transient voltage-dependent outward potassium current in mammalian cerebellar Purkinje cells. *Brain Res.* 567:153–158.
Wickens J (1997) Basal ganglia: structure and computations. *Network* 8:R77–R109.
Willms AR, Baro DJ, Harris-Warrick RM, and Guckenheimer J (1999) An improved parameter estimation method for Hodgkin-Huxley models. *J. Comp. Neurosci.* 6:145–168.
Wood SN, and Thomas MB (1999) Super-sensitivity to structure in biological models. *Proc. R. Soc. Lond. B.* 266:565–570.
Yamada WM, Koch C, and Adams PR (1998) Multiple channels and calcium dynamics. In: I. Segev and C. Koch, eds. Methods in Neuronal Modeling. 2nd ed. MIT Press, Cambridge, Mass. pp 137–170.
Yoshida A, Oda M, and Ikemoto Y (1991) Kinetics of the Ca^{2+}-activated K^+ channel in rat hippocampal neurons. *Jap. J. Physiol.* 41:297–315.

Appendix A

The formal descriptions of the different PC cell models studied are now given.

Model 1

The principal equation used to describe V_m was

$$C_m \frac{dV(t)}{dt} + I_{Nap} + kI_{Cap} + I_{leak} + I_{Klump} + I_{Glu} + I_{inj} = 0. \tag{1}$$

where I_{Nap} was a persistent sodium current, I_{Cap} was a high-threshold P-type calcium current, I_{leak} a leak current that returned V_m to V_r, I_{Klump} was a lumped potassium current that repolarized the action potential and generated the relative refractory period, I_{Glu} the synaptic glutamate current and I_{inj} the injected current. In the case of I_{Cap}, k was a constant proportional to I_{inj}. Unless otherwise stated, a general equation obtained from Ohm's law

$$I = \bar{g}g(t)(V_m(t) - E_r) \tag{2}$$

defined each current through the time-dependent membrane and/or synaptic conductance $g(t)$, scaled by the maximum conductance for the channel $\bar{g}$. Here, $g(t)$ took the form of an alpha function of time

$$g(t) = \alpha T e^{-\alpha T}, \tag{3}$$

where $\alpha = \tau_m / t_{peak}$ and $T = (t - t_0)/\tau_m$ (Rall, 1967). For I_{Nap} and I_{Cap},

$$g(t) = \begin{array}{ll} ((V_m(t) - V_{th})/(V_{max} - V_{th}))(V_m(t) - E_r) & \text{if } V_m(t) \geq V_{th}, \\ 0 & \text{if } V_m(t) < V_{th}, \end{array} \tag{4}$$

where V_{th} was the voltage threshold for activation of the conductance and V_{max} was the V_m at which the maximum current was reported to occur. A passive leak current through a time- and voltage-independent conductance was given by

$$I_{leak} = g_{leak}(V_m(t) - E_{leak}). \tag{5}$$

The Nernst potential for E_{Ca} was not calculated for this model.

Model 2

The principal equation used to describe V_m was

$$C_m \frac{dV(t)}{dt} + I_{Naf} + I_{Nap} + kI_{Cap} + I_{Kdr} + I_{Kh} + I_{Km} + I_{Ka} + I_{Kc} + I_{K2} + I_{Glu} + I_{inj} = 0 \quad (6)$$

where I_{Naf} was the fast sodium current, I_{Nap} was a persistent sodium current, I_{Cap} was a high-threshold P-type calcium current, I_{Kdr} the potassium delayed rectifier, I_{Kh} was the potassium anomalous rectifier, I_{Km} the persistent potassium current, I_{Ka} the potassium A current, I_{Kc} and I_{K2} the BK- and K2-type calcium-activated potassium currents, respectively, I_{Glu} the synaptic glutamate current and I_{inj} the injected current.

This model provided a much more detailed representation of a PC than the previous model by employing rate functions described by the HH formalism. Here, when the voltage-dependent values of the forward (α_y) and backward (β_y) rate functions for the gating variable y are known, the steady-state conductance is given by

$$y_\infty = \alpha_y / (\alpha_y + \beta_y), \quad (7)$$

the time constant of relaxation (to y_∞) by

$$\tau_y = 1/(\alpha_y + \beta_y), \quad (8)$$

and the kinetic equation for y becomes

$$\frac{dy(t)}{dt} = (y_\infty(U) - y)/\tau_y(U), \quad (9)$$

where U is the value $V_m(t)$ of the compartment containing the conductance of interest, and τ_y a time constant. By substitution for y_∞ and τ_y in Eq. (9) the general HH scheme for describing the temporal behavior of the voltage- and time dependent activation ($y = m$) and inactivation ($y = h$) gates controlling current flow through a conductance is obtained,

$$\frac{dy(t)}{dt} = \alpha_y(1 - y) - \beta_y y. \quad (10)$$

In the HH formulation $g(t)$ is given by the product of the maximum channel conductance, voltage-dependent activation gates, voltage-dependent inactivation gates, and concentration-dependent activation gates (typically Ca^{2+}-sensitive) and becomes

$$g(V_m, [Ca^{2+}]_i, t) = \bar{g} m^p(V_m, t) h^q(V_m, t) z^r([Ca^{2+}]_i, t), \quad (11)$$

where p, q and r are exponents that influence the amplitude time course of the conductance. Thus, Eq. (11) gives the probability of finding a certain number (p) of voltage-dependent activation gates (m) open, a certain number of voltage-dependent inactivation gates (h) not closed, and when appropriate the number (r) of concentration-dependent activation gates (z) open, and therefore the total normalized channel conductance.

Alternatively, we obtained y_∞ directly from a Boltzmann style "steady-state" (in)activation curve,

$$y_\infty(V_m) = \frac{\phi}{1 + e^{(V_m - V_{0.5})/\delta}}, \tag{12}$$

where $V_{0.5}$ was the voltage at which half-maximal activation occured, ϕ the maximal probability of activation (assumed to be 1), and δ the slope factor related to the valence of charge that must be displaced for the channel to switch between closed and open states. Once obtained, y_∞ was substituted into equation (9) and the standard form of the current equation was given by Eq. 11.

The change in intracellular calcium concentration was modelled as

$$\frac{d[Ca^{2+}]_i}{dt} = \frac{-I_{Cap}}{zFv_i} - B([Ca^{2+}]_i - [Ca^{2+}]_{min}) \tag{13}$$

where z is the number of charges per ion (2 for Ca^{2+}), F Faraday's constant (9.649×10^4 Coulombs/mole), v_i the volume of the intracellular shell occupied by calcium ions, B a constant that lumped together many different mechanisms known to reduce $[Ca^{2+}]_i$ including buffering and diffusion, and $[Ca^{2+}]_{min}$ the resting calcium concentration (50 nM, Llano et al., 1994) (see De Schutter and Smolen, 1998). The value of the calcium equilibrium potential (E_{Ca}, initially 142 mV) was then updated at each time step with the Nernst equation

$$E_{Ca} = \frac{RT}{zF} ln \frac{[Ca^{2+}]_o}{[Ca^{2+}]_i} \tag{14}$$

where R is the gas constant (8.32), T the absolute temperature ($310\,^\circ K$), z as given above for Eq. (13) and $[Ca^{2+}]_o$ was assumed to be a constant 2 mM.

Model 3

The only differences between Models 1 and 3 were the (i) adjustment of the principal equation (Eq. 1) to give the V_m for each of two compartments, (ii) the partition of C_m between the somatic ($C_{ms} = f_{cm} \times C_m$) and dendritic ($C_{md} = 1 - C_{ms}$) compartments, and (iii) the introduction of a coupling conductance (G_i) to connect them,

$$C_{ms}\frac{dV_s(t)}{dt} + I_{Nap} + I_{leak} + I_{Klump} + kI_{Caps} + I_{Glu_s} + I_{inj} - G_i(V_d - V_s) = 0 \tag{15}$$

$$C_{md}\frac{dV_d(t)}{dt} + kI_{Capd} + I_{Glud} - G_i(V_s - V_d) = 0. \tag{16}$$

The Nernst potential for E_{Ca} was not calculated for this model.

Model 4

Similarly, the only differences between Models 2 and 4 were equivalent to those just outlined for Models 1 and 3. In Model 4 the representation of the PC cell given for Model 2 was extended by (i) the addition of a second compartment with the currents distributed appropriately between the somatic compartment and dendritic compartments, (ii) the partition of

C_m between C_{ms} and C_{md} as given above for Model 3, and (iii) the introduction of a coupling conductance (G_i) to connect these two compartments.

$$\begin{aligned} C_{ms}\tfrac{dV_s(t)}{dt} &+ I_{Naf} + I_{Nap} + kI_{Caps} + I_{Kdr} + I_{Khs} + \\ &I_{Kms} + I_{Kas} + I_{Kc} + I_{Glus} + I_{inj} - G_i(V_d - V_s) = 0 \end{aligned} \quad (17)$$

$$C_{md}\frac{dV_d(t)}{dt} + kI_{Capd} + I_{Kmd} + I_{Kad} + I_{K2} + I_{sAHP} + I_{Glud} - G_i(V_s - V_d) = 0. \quad (18)$$

APPENDIX B

The equations describing the kinetics of channel gating for each of the PC conductances are now given. As mentioned in the Methods section the values in the following equations have been adjusted for 37 °C. With the exception of the translation of $\hat{z}_\infty$ by $\hat{z}$ in the calculation of $\bar{g}_{K2}$ by Eq. (45), all the following parameter values were obtained from the literature as referenced in the Methods section for the single-compartment HH-based PC (Model 2).

The Fast Sodium Current (I_{Naf})

The fast sodium current was

$$I_{Naf} = \bar{g}_{Naf} m^3 h (V_m - E_{Na}), \quad (19)$$

where the activation variable (m) was given by Eq. (10) and the forward (α_m) and backward (β_m) rate constants were

$$\alpha_m(V_m) = \frac{35.0}{\exp^{-(V_m+5.0)/10.0}} \quad \text{and} \quad \beta_m(V_m) = \frac{7.0}{\exp^{(V_m+65.0)/20.0}}. \quad (20)$$

Similarly, the inactivation variable (h) was given by Eq. (10) where the forward (α_h) and backward (β_h) rate constants were

$$\alpha_h(V_m) = \frac{0.225}{\exp^{(V_m+80.0)/10.0}} \quad \text{and} \quad \beta_h(V_m) = \frac{7.5}{\exp^{-(V_m-3.0)/18.0}}. \quad (21)$$

The Persistent Sodium Current (I_{Nap})

The persistent sodium current was

$$I_{Nap} = \bar{g}_{Nap} m^3 (V_m - E_{Na}), \quad (22)$$

where m was given by Eq. (9),

$$m_\infty(V_m) = \frac{1.0}{1.0 + \exp^{(V_m+41.6)/3.8}} \quad (23)$$

and τ_m was set to 0.8 ms.

The P-Type Calcium Current (I_{Cap})

The P-type calcium current was

$$I_{Cap} = \bar{g}_{Cap} m (V_m - E_{Ca}), \tag{24}$$

where m was given by Eq. (10) and α_m and β_m were

$$\alpha_m(V_m) = \frac{42.5}{1.0 + \exp^{-(V_m - 8.0)/-12.5}} \quad \text{and} \quad \beta_m(V_m) = \frac{175.0}{1.0 + \exp^{(V_m + 74.0)/14.5}}. \tag{25}$$

Similarly, h was given by Eq. (10) where α_h and β_h were

$$\alpha_h(V_m) = \frac{0.0075}{1.0 + \exp^{(V_m + 29.0)/8.0}} \quad \text{and} \quad \beta_h(V_m) = \frac{0.00275}{1.0 + \exp^{-(V_m + 23.0)/-8.0}}. \tag{26}$$

The effect of calcium influx and buffering on $[\mathrm{Ca}^{2+}]_i$ and E_{Ca} was calculated independently for the somatic and dendritic compartments of the two-compartment PC from Eq. (13) and the Nernst Eq. (14) at each timestep, assuming v_{is} and v_{id} as given in Table 2.

The Anomalous Potassium Rectifier (I_{Kh})

The anomalous potassium rectifier current was

$$I_{Kh} = \bar{g}_{Kh} m (V_m - E_r), \tag{27}$$

where E_r was -30 mV and m was the sum of a fast and a slow activation variable

$$\frac{dm(t)}{dt} = \frac{0.8 m_\infty - m}{39.0} + \frac{0.2 m_\infty - m}{272.0}, \tag{28}$$

where

$$m_\infty = \frac{1.0}{1.0 + \exp^{(V_m + 82.0)/7.0}}. \tag{29}$$

The Delayed Potassium Rectifier (I_{Kdr})

The delayed rectifying potassium current was

$$I_{Kdr} = \bar{g} K_{dr} m^2 h (V_m - E_K), \tag{30}$$

where m was given by Eq. (9) and m_∞ and τ_m took their normal forms from equations (7) and (8), respectively, where

$$\alpha_m(V_m) = \frac{-0.0235(V_m - 8.0)}{\exp^{(V_m - 8.0)/12.0} - 1.0} \quad \text{and} \quad \beta_m(V_m) = 5.0 \exp^{-(V_m + 127.0)/30.0}. \tag{31}$$

Similarly, the inactivation variable h was given by Eq. (9) where

$$h_\infty = \frac{1.0}{1.0 + \exp^{(V_m + 25.0)/4.0}} \text{ and } \tau_h = \begin{array}{ll} 1,200 & \text{if } V_m < -25.0, \\ 10 & \text{if } V_m \geq -25.0. \end{array} \tag{32}$$

The Persistent Potassium Current (I_{Km})

The persistent potassium current was

$$I_{Km} = \bar{g}K_m(V_m - E_K) \tag{33}$$

where m was given by Eq. (9) with

$$m_\infty = \frac{1.0}{1.0 + \exp^{-(V_m+35.0)/10.0}} \quad \text{and} \quad \tau_m = \frac{220.0}{3.3\exp^{(V_m+35.0)/20.0} + \exp^{-(V_m+35.0)/20.0}}. \tag{34}$$

The Potassium A Current (I_{Ka})

The potassium A current was a composite of m_∞ and h_∞ from Wang et al. (1991) and τ_m and τ_h from De Schutter and Bower (1994a). This approach was supported by the fact that Wang et al. (1991) gave a value for τ_h (95 ms), but not for τ_m, that was in reasonable agreement with De Schutter and Bower (1994a) for V_m more hyperpolarized than V_r. Further, the data reported by Wang et al. (1991) was for the rat. Consequently, the potassium A current was

$$I_{Ka} = \bar{g}K_a m^4 h(V_m - E_K), \tag{35}$$

where m was given by Eq. (9) with

$$m_\infty = \frac{1.0}{1.0 + \exp^{-(V_m+38.5)/5.4}} \tag{36}$$

and τ_m given by Eq. (8) with

$$\alpha_m(V_m) = \frac{1.4}{1.0 + \exp^{-(V_m+27.0)/12.0}} \quad \text{and} \quad \beta_m(V_m) = \frac{0.49}{1.0 + \exp^{(V_m+30.0)/4.0}}. \tag{37}$$

Similarly, h was given by Eq. (9) where

$$h_\infty = \frac{1.0}{1.0 + \exp^{(V_m+64.8)/8.1}} \tag{38}$$

and τ_h was given by Eq. (8) where

$$\alpha_h(V_m) = \frac{0.0175}{1.0 + \exp^{(V_m+50.0)/8.0}} \quad \text{and} \quad \beta_h(V_m) = \frac{1.3}{1.0 + \exp^{-(V_m+13.0)/10.0}}. \tag{39}$$

The BK-Type Calcium-activated Potassium Current (I_{Kc})

The high threshold BK-type calcium-activated potassium current was

$$I_{Kc} = \bar{g}K_c mz(V_m - E_K), \tag{40}$$

where m was given by Eq. (9) with

$$\alpha_m(V_m) = 7.5 \quad \text{and} \quad \beta_m(V_m) = \frac{0.11}{\exp^{(V_m-35.0)/14.9}}. \tag{41}$$

The calcium-dependent activation gate z was given by Eq. (9) where

$$z_\infty = 1.0/\{1.0 + 180.0(1270/0.95[Ca^{2+}]_i^2 + 1.0)/2905\}, \qquad \tau_z = 10.0 \tag{42}$$

and $[Ca^{2+}]_i$ was calculated directly from I_{Cap} by

$$\frac{d[Ca^{2+}]_i}{dt} = \frac{-5.181 \times 10^6 I_{Cap}}{v_i} - B([Ca^{2+}]_i - [Ca^{2+}]_{min}), \tag{43}$$

where the constant -5.181×10^6 converted current (μA), time (ms), and volume (μm^3) to concentration (μM), v_i was the shell volume and B was a calcium buffer/diffusion factor with the value of 4700 in the one-compartment PC, and either 470 or 4700 in the soma and dendrites, respectively, of the two-compartment PC.

The K2-Type Calcium-activated Potassium Current (I_{K2})

The K2-type low-threshold calcium-activated potassium current was

$$I_{K2} = \bar{g}K_2 m\hat{z}(V_m - E_K), \tag{44}$$

where the activation variable m was given by Eq. (9) with

$$\alpha_m(V_m) = 25.0 \qquad \text{and} \qquad \beta_m(V_m) = \frac{0.11}{\exp^{(V_m+5.0)/10.0}}. \tag{45}$$

The calcium-dependent activation gate z was given by Eq. (9) where the calcium sensitivity of gK_2 was increased by reducing the value calculated for z_∞ from Eq. (42) by the translation $\hat{z}_\infty = \exp^{-3.5} z_\infty$ and $[Ca^{2+}]_i$ given by appropriately substituting for I_{K2} in Eq. (43).